PARAMETRIC STUDY OF THE TOWLINE SHAPE OF AN AIRCRAFT DECOY

THESIS

Tyler L. Richardson, Ensign, USNR

AFIT/GAE/ENY/05-J08

DEPARTMENT OF THE AIR FORCE
AIR UNIVERSITY

AIR FORCE INSTITUTE OF TECHNOLOGY

Wright-Patterson Air Force Base, Ohio

AFIT/GAE/ENY/05-J08

PARAMETRIC STUDY OF THE TOWLINE SHAPE OF AN AIRCRAFT DECOY

THESIS

Presented to the Faculty

Department of Aeronautics and Astronautics

Graduate School of Engineering and Management

Air Force Institute of Technology

Air University

Air Education and Training Command

In Partial Fulfillment of the Requirements for the

Degree of Master of Science in Aeronautical Engineering

Tyler L. Richardson, BSE

Ensign, USNR

June 2005

AFIT/GAE/ENY/05-J08

PARAMETRIC STUDY OF THE TOWLINE SHAPE OF AN AIRCRAFT DECOY

Tyler L. Richardson, BSE
Ensign, USNR

Approved:

/signed/

_____ _____
Prof. Ralph Anthenien (Chairman) date

/signed/

_____ _____
Lt Col Raymond Maple (Member) date

/signed/

_____ _____
Prof. Mark Reeder (Member) date

Abstract

Some of today's aircraft use decoys as a defense against enemy weapons. The decoy is towed behind the aircraft with the intention of attracting the weapon propagator by deception, trying to mislead the weapon into detecting it instead of the aircraft. An aircraft deploys a decoy via a towline extending out behind and below the aircraft. However, during some maneuvers, the towline moves up into the jet exhaust plume of the aircraft. The high temperatures of the exhaust can cause damage to the towline cable, ranging from disrupting data flow between the decoy and aircraft to severing the towline altogether. This research modeled the system to determine the towline shape and position relative to the aircraft under steady state conditions. Non-dimensional parameters were utilized in order to investigate what parameter groups effect the motion of the towline, reducing the steady state solution space from 7 parameters to 2 parameters. The effect of both parameter groups in determining the shape of the towline was studied, and recommendations for preventing the towline from entering the jet exhaust during straight and level flight were made.

To Mom and Dad, for all that you have done,

and to my fiancé, for your patience, encouragement,

love, and support throughout this work

Acknowledgements

I would like to express my deepest gratitude to my thesis advisor, Dr. Ralph Anthenien. His guidance and support are what made this possible. His time and effort are greatly appreciated.

Tyler L. Richardson

Table of Contents

List of Figures

Figure Page

Page

List of Tables

Table Page

PARAMETRIC STUDY OF THE TOWLINE SHAPE OF AN AIRCRAFT DECOY

I: Introduction and Background

Aircraft Survivability

The use of the airplane in combat is a relatively new concept given the long history of armed conflict. However, the evolution process that combat aircraft have undergone has occurred at a rapid rate and, when observing aircraft today, it is easy to forget that the military only began using the airplane at the beginning of the twentieth century. From first getting airplanes into the air, to enhancing performance, to designing for survivability, military aviation has come a long way in a short period of time.

In the early days the military benefited from the ability to merely obtain flight. Flight provided a new offensive weapon, and, more importantly at that time, a strategic tool when used for observation and reconnaissance from above. These first aircraft were hard to maintain and were not very survivable, which is not surprising since the concept was brand new. Military aircraft became more survivable as a direct result of improvements made to the airplane. They were better manufactured with improved designs as progress was made in aviation science. Advances were made in propulsion systems and airplanes were flying faster and higher year after year. Up until the 1970's, survivability was a matter of the performance of the aircraft – the faster and higher an aircraft could fly the more likely it was to survive in combat. So, naturally, most

development was focused on increasing performance. Soon it was determined that this was not the only way to improve the survivability of military aircraft, and in the 1970's survivability developed into its own engineering design discipline (Ball, 2003:xix).

Aircraft survivability is a measure of the ability of an aircraft "to avoid or withstand a man-made hostile environment" (Ball, 2003:1). One can deduce from this definition that the survivability discipline is divided into two areas – one concerned with avoiding a hostile environment and the other primarily focusing on withstanding the hostile environment. When an aircraft is ill-suited to avoid a threat, it is said to be susceptible to that threat (Ball, 2003:1). Susceptibility reduction, therefore, is a major contributor to aircraft survivability. On the other hand, when an aircraft comes in contact with a threat it cannot withstand, the aircraft is said to be vulnerable to that threat (Ball, 2003:1). It follows that vulnerability reduction is the other major contributor to survivability. The survivability discipline has developed an extensive list of ways to reduce both susceptibility and vulnerability. This research dealt with one particular method of susceptibility reduction – the use of a towed decoy.

Susceptibility Reduction with a Towed Decoy

Many combat aircraft are capable of deploying a decoy while in flight. The decoy is towed behind the aircraft with a towline. A typical towed decoy system is shown in Figure 1, along with other susceptibility reduction techniques. Many different types of decoys can be used at the end of the towline, but they all share one common goal: reduce the susceptibility of the towing aircraft. The decoy helps the aircraft avoid a threat (i.e.

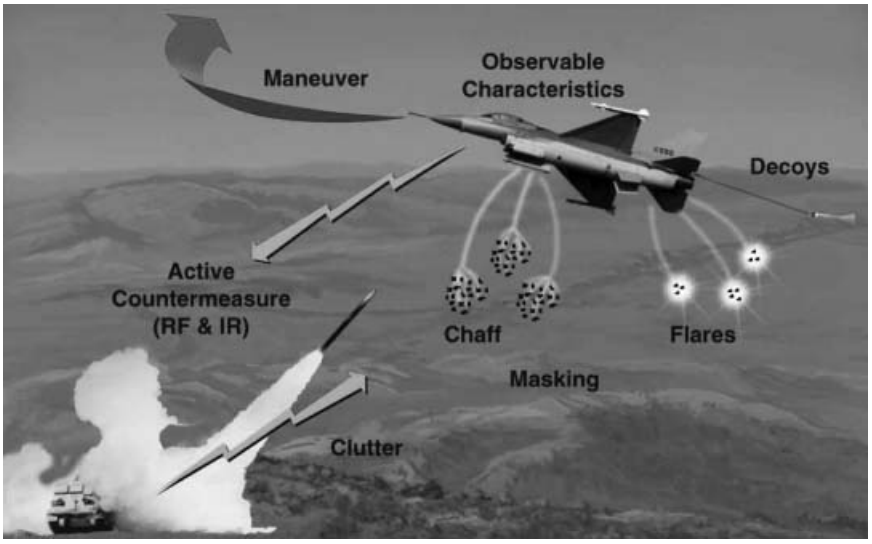

(used without permission) **(Ball, 2003:165)**

Figure 1. Towed Decoy System with Other Susceptibility Reduction Techniques

an enemy missile) by deceiving the threat into attacking it rather than the aircraft. This aids against threats that have been able to detect and fire at the aircraft.

Various decoys achieve this goal in different ways, according to the type of threat they are intended to counter. A decoy designed to deceive a radar guided missile presents a more attractive radar cross section than the cross section of the host aircraft to the guidance system of the missile. As a result, the missile will be guided to the decoy rather than the aircraft. Some of these decoys emit signals they generate themselves to accomplish the radar deception, while others use a countermeasures device onboard the towing aircraft to generate the signals (Ball, 2003:580). When the latter type of decoy is used, the countermeasures device and the decoy are linked by a fiber-optic cable that is part of the towline. Some of these decoys can be retrieved for future use and some cannot, depending on the system. Another type of decoy attempts to deceive infrared guided threats. In this case the decoy puts forth an attractive infrared signature that will

again lure the threat away from the aircraft and to itself. The decoy is able to mimic the radiation given off by the engine exhaust plume of the aircraft by "slowly dispensing a pyrophoric material in a plume" (Ball, 2003:583). The idea, then, is that the guidance system of the threat tracks the infrared radiation of the decoy rather than the engine exhaust of the aircraft, and the aircraft avoids the threat.

Using a towed decoy to reduce the susceptibility of an aircraft is an important method for increasing the survivability of the aircraft. This method has many advantages, one of which is the relative ease of implementation that these systems provide. Aircraft do not need to undergo extensive modifications to tow a decoy, nor does the system need to be designed into the aircraft while they are still on the drawing board. This enables the towed decoy system to be added to aircraft lacking susceptibility reduction. These can be older aircraft that were not designed with susceptibility reduction in mind, or newer aircraft that can benefit from an additional reduction in susceptibility. Another advantage is the low cost of a system comprised of a towline and an expendable decoy. The fact that the decoys are referred to as *expendable* is an indication of their relatively low cost. Should the decoy lure an incoming missile away from the aircraft and be destroyed, there would be no comparison between the cost of losing the decoy and the cost of losing the aircraft and crew.

The importance of aircraft survivability has continued to grow through the years. For one reason, the public view of casualties in battle has changed during the conflicts of the twentieth century. During World War II the United States and the United Kingdom lost around 50,000 aircraft (Ball, 2003:86). This number was drastically reduced during the Southeast Asia conflict, where the United States lost a total number of aircraft near

8500 (Ball, 2003:86). Finally, in Desert Storm the United States managed to only suffer 27 aircraft losses in total (Ball, 2003:87). While any loss of life (though the loss of an aircraft doesn't necessarily translate into the loss of life) is a horrible consequence of war, these dramatic improvements in survivability of United States aircraft are quite an accomplishment. With the decrease in casualties has come the higher expectation from the public that all casualties should be able to be avoided, or nearly all of them. Thus, survivability needs to always be considered and continually improved. A towed decoy is one way to do that. The political ramifications of a downed aircraft are also greater today than in the past. The importance of aircraft survivability, and thus survivability enhancements like the towed decoy, is quite clear.

The Problem At Hand

The towed decoy system is not perfect and some issues have been encountered during its use. Under normal flight conditions the decoy is behind and below the towing aircraft, and so is the towline. This is where the decoy and towline are designed to be. However, the towline does not always stay directly behind and below the aircraft during flight operations. Some flight maneuvers have caused the towline near the aircraft to move into the jet engine exhaust plume. The high temperature of the engine exhaust can cause varying amounts of damage. Some damage has been the disruption of the data link – if the decoy is active – between the decoy and the aircraft, which reduces the decoy to a towed brick since it would not be emitting any radar signals. More severe damage has

included the severing of the towline, resulting in the loss of the decoy (possibly without a threat ever encountered).

In order for the towed decoy to be useful and increase the survivability of the aircraft, it has to be able to be towed during typical flight maneuvers and remain attached, undamaged, and useable. The purpose of this research is to begin the process of three-dimensional, transient modeling of the towline using a computer. This will allow engineers to determine the shape of the towline under various flight conditions without the cost and difficulty of flight testing. It will also provide a tool for studying what characteristics of the towline and its environment affect the shape of the towline and where it is relative to the aircraft, and in what manner those characteristics affect the shape and position of the towline. The research described in the following chapters will serve as a stepping stone for future work in this area.

The next chapter will discuss the research completed by others relevant to this problem and indicate what can be applied to the towed decoy system. This research includes towed systems in both air and water. Chapter III will describe the method used to conduct the present research, which will include the derivation of the equations of motion of the towline, the nondimensionalization of the system and isolation of the important groups of parameters, as well as the procedure of numerical integration used to solve the equations. The results of the research will be discussed in Chapter IV and many illustrations of towline shapes will be provided for the appropriate range of values for the nondimensional groups. This will allow conclusions to be drawn in Chapter V about the affect of each individual nondimensional group on the shape of the towline, as well as the position relative to the aircraft. Recommendations for preventing the towline from going

into the engine exhaust plume based on the results of this research will also be offered here, along with recommendations for future work.

II. Past Research

Some research that has already been completed is related to the present study. In particular, papers published by Schram and Reyle, Skop and Choo, Narkis, Kang and Latorre, and Buckham, Nahon, and Seto, as well as a thesis by Barnes and Pothier, all investigate a towed system in one way or another. This chapter will highlight their work and describe how it relates to and/or is different from this research.

Schram and Reyle

In 1968 in "A Three-Dimensional Dynamic Analysis of a Towed System", Schram and Reyle described their work dealing with a ship towing a submerged body. To investigate the motion of the system, they first derived the equations of motion. They applied a coordinate transformation from the space reference axes to coordinate axes aligned with the towline element (Schram and Reyle, 1968:215). For boundary conditions they noted that "the towline at its point of attachment to the towing ship must have the same motion as the ship" (Schram and Reyle, 1968:216). Similar boundary conditions at the submerged body end of the towline were used, forcing the towline at that end to have the same motion as the submerged body. Schram and Reyle were able to make relevant conclusions from their numerical solution of the system. One, there is a coupling between the longitudinal motion along the towline and the transverse motion. They found "that longitudinal disturbances generate transverse motion and vice versa, when the towline is not straight" (Schram and Reyle, 1968:219). Another conclusion

dealt with their transfer function and how it changed with different system characteristics. The transfer function described the motion of the submerged body resulting from the motion of the ship. The transfer function was the ratio of the amplitudes of these two motions – body motion to ship motion (Schram and Reyle, 1968:220). Schram and Reyle discovered that as the length of the towline increased, the transfer function decreased, speculating that this was a result of more damping experienced by the longer towline (Schram and Reyle, 1968:220). A similar relationship was observed between the towing speed and the transfer function as increased towing speed resulted in a decreased transfer function. With increased speed the pitch angle of the towline was decreased, which meant that more of the motion was of transverse nature than longitudinal. Schram and Reyle determined that transverse motion was subject to more damping than longitudinal motion, explaining the observed decrease in the transfer function (Schram and Reyle, 1968:220).

The research by Schram and Reyle provides some insight into a way to approach the problem of modeling the towed decoy system. Their conclusions of what happens with increasing towing speed and increasing towline length offer the results of this research a comparison. At the same time, there are differences between the ship towing a submerged body and an aircraft towing a decoy. The towline moves through water in the former but is subject to air in the latter, and the towing vehicle in the former remains on the surface of the water at a constant altitude while in the latter the towing vehicle can climb and descend to change altitude.

Barnes and Pothier

Barnes and Pothier completed a thesis titled "Wind Tunnel Measurement of Airborne Towed Cable Drag Coefficients" in 1971. They studied the drag characteristics of four cables used in towing operations at the time of their writing. Of particular relevance, their work included the *cross flow principal* which says "the dynamic pressure acting on an inclined cylinder is a function of the airflow component normal to the cylindrical axis" (Barnes and Pothier, 1971:41). This principal is illustrated in Figure 2 where a cylinder in an airstream is inclined at an angle α.

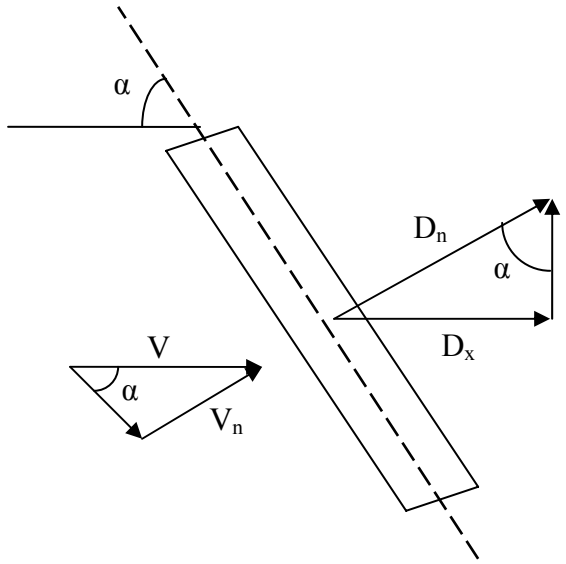

Figure 2. Inclined Cylinder in Freestream

The airflow normal to the axis of the cylinder is V_n, according to

$$V_n = V \sin \alpha \tag{1}$$

where V is the velocity of the freestream. The definition of the drag normal to the cylindrical axis is

$$D_n = C_d\left(\frac{1}{2}\rho_a V_n^2\right)d_c l \tag{2}$$

where C_d is the coefficient of drag of the cylinder, ρ_a is the density of air, l is the length of the cylinder, and d_c is the diameter of the cylinder (Barnes and Pothier, 1971:42). Substituting Equation 1 into Equation 2 gives

$$D_n = \frac{1}{2}C_d\rho_a d_c l V^2 \sin^2\alpha \tag{3}$$

Returning to Figure 2, the component of drag in the direction of the freestream can be determined using

$$D_x = D_n \sin\alpha = \frac{1}{2}C_d\rho_a d_c l V^2 \sin^3\alpha \tag{4}$$

The *cross flow principle* dictates that in order to calculate the drag of an inclined cylinder in the direction of the freestream, the coefficient of drag needs to be multiplied by the cube of the sine of the angle of attack (Barnes and Pothier, 1971:43).

The work done by Barnes and Pothier will be used in this work when deriving the equations of motion. Specifically, the *cross flow principle* will be applied when determining the components of drag of the towline in the x, y, and z-directions. The component of drag in the y-direction will also be referred to as the lift generated by the towline.

Skop and Choo

"The Configuration of a Cable Towed in a Circular Path", a paper published by Skop and Choo in 1971, investigated what parameters of a towed system affect the

equilibrium state of the system. Their work can be applied to any towing medium, such as air or water. To begin deriving the equilibrium equations, Skop and Choo defined a Cartesian coordinate system for their problem that rotated with the point on the towing vehicle where the towline was attached (Skop and Choo, 1971:856). This was beneficial because of their specific study of a towed body in a circular path. They also chose to neglect tangential and side components of drag, and restricted their towed body to a spherical drogue (Skop and Choo, 1971:857). Skop and Choo decided to nondimensionalize the equilibrium equations and boundary conditions to isolate the combinations of parameters important to the equilibrium system (Skop and Choo, 1971:858). Specifically, they wanted to study the equilibrium position of the towed body because certain values of the system parameters led to an equilibrium position close to the axis of rotation. Taking advantage of this would allow fixed-wing aircraft to make pinpoint deliveries simply by flying a circular path (Skop and Choo, 1971:856). Their work determined the ranges of the combinations of system parameters that led to the desired equilibrium position of the towed body.

Despite being a simplified version, the work done by Skop and Choo relates to the present research. The present work will not be limited to a circular flight path, but a comparable nondimensional approach will be used in order to determine similar conclusions about the system parameters.

Narkis

Narkis published "Approximate Solution for the Shape of Flexible Towing Cables" in 1977. In his work, Narkis examined the two-dimensional case of an aircraft

towing a body. He included drag in the x-direction and lift in the y-direction in developing his equilibrium equations of motion. Since Narkis was concerned with the steady state solution, he was able to start the numerical integration of his system of equations at the towed body end of the towline and work his way up to the aircraft (Narkis, 1977:924). He was also content with approximate shapes of the towline because he thought the position of the towed body was more important than the shape of the towline. In fact, Narkis felt "the exact shape of the cable is of less importance than the vertical separation and horizontal distance between the towing aircraft and the towed vehicle, and the maximal tension in the cable" (Narkis, 1977:925).

The approach used by Narkis to develop his two-dimensional solution is similar to the approach used in this research to develop a three-dimensional solution. The steady state solution will integrate numerically from the decoy up to the aircraft. However, integrating in the reverse direction, from the aircraft down to the decoy, will also be investigated in this research because this is the direction of integration necessary for the transient solution. Unlike the work by Narkis, the present study will focus on the shape of the towline and not as much on the location of the decoy, as the position of the towline relative to the aircraft engine exhaust has lead to the need for the present research.

Kang and Latorre

In 1991, Kang and Latorre wrote "Aerodynamics Modeling of Towed-Cable Dynamics". Their goal was to produce a transient model of a towed system, but limited their model to circular flight paths (Kang and Latorre, 1991:2). In particular, they

investigated what they called the *yo-yo phenomenon*, or oscillatory behavior of the towed body (Kang and Latorre, 1991:1). With this in mind, their results mainly discussed the motion of the towed body and less emphasis was put on the shape of the towline. The paper included a thorough literature survey and examined available computer codes used to model underwater towed systems.

The literature review was beneficial to this present research. As evidence, some of the papers discussed above were included in the review. The present work will aim at modeling the towline accurately and not specialize in describing the motion of the towed body. As noted before, this work will not be restricted to circular flight paths but will apply to straight and level flight and, eventually, typical flight maneuvers.

Buckham, Nahon, and Seto

A paper written in 1999 by Buckham, Nahon, and Seto titled "Three-Dimensional Dynamics Simulation of a Towed Underwater Vehicle" extended work that had been done in two-dimensions to three-dimensions (Buckham and others, 1999:91). The work used a lumped mass model of the towline and included a specific towed body at the end of the towline. The towed body had active control surfaces, including a wing above the hull and aft fins configured in an X (Buckham and others, 1999:91). Buckham, Nahon, and Seto outline their derivation of the equations of motion for their underwater system and describe how the active control surfaces affect the system. They also explain their method of numerical integration of the system of equations. The solution was tested by

simulating a 180º turn by the towing ship and comparing their results to test data. The comparison was favorable (Buckham and others, 1999:98).

Unfortunately the underwater nature of the research completed by Buckham, Nahon, and Seto limits how much can be applied to the present work. In addition, the inclusion of the actively controlled towed body makes the equations specific to their case and the results cannot be compared to the results of the present research. On the other hand, the derivation of the equations of motion and the development of the system of first order differential equations to be numerically integrated can be applied to this work.

Applicable Past Research Summary

As can be seen, towed system research is not new, but little has been investigated for aircraft flying in noncircular flight paths. Underwater towed systems have had the largest amount of successful research, and some of what has been learned there can be applied to aerial towed systems. Some of the past research investigated the two-dimensional case, while some examined the motion of the towed body with less concern about the towline, and others studied the system constrained by a towing aircraft in a circular flight path. The present work will extend this past research to the three-dimensional case, accurately model the shape of the towline, and study the straight and level flight path case, eventually leading to no restrictions on the flight path of the towing aircraft.

III: Method

This research will develop the equations of motion of the towed decoy system and determine the governing differential equations. The derivation will be original work, using the derivations completed in the past work used only as a basis. These equations will be nondimensionalized to uncover the important parameter groups that define the shape of the towline. This will be the first time that these groups have been isolated and investigated in this manner. The differential equations will then be integrated numerically to obtain the shape and position of the towline relative to the aircraft.

Equations of Motion

To start the derivation of the equations of motion, coordinate axes need to be defined. The positive x-axis will be defined here as out the front of the aircraft, the positive y-axis will be out the top of the aircraft, and the positive z-axis will be out the right wing of the aircraft. Figure 3 shows the coordinate axes and also defines the two angles used in the equations. The polar angle from the x-axis is denoted as α and the azimuthal angle in the yz-plane from the y-axis is denoted as ϕ. From Figure 3 we can see that

$$dx = dl\cos\alpha \tag{5}$$

$$dy = dl\sin\alpha\cos\phi \tag{6}$$

$$dz = dl\sin\alpha\sin\phi \tag{7}$$

where *dl* is the elemental length of the towline described as

$$dl = \sqrt{dx^2 + dy^2 + dz^2} \tag{8}$$

Since, in the end, we will want to integrate the system of differential equations, it is best to have all the trigonometric functions in the equations in terms of first order derivatives with respect to *dl*. Thus, Equation 5 can be expressed as

$$\cos\alpha = \frac{dx}{dl} \tag{9}$$

Also, from Figure 3 we can see that

$$dl \sin\alpha = \sqrt{dy^2 + dz^2} \tag{10}$$

which can be rewritten as

$$\sin\alpha = \sqrt{\left(\frac{dy}{dl}\right)^2 + \left(\frac{dz}{dl}\right)^2} \tag{11}$$

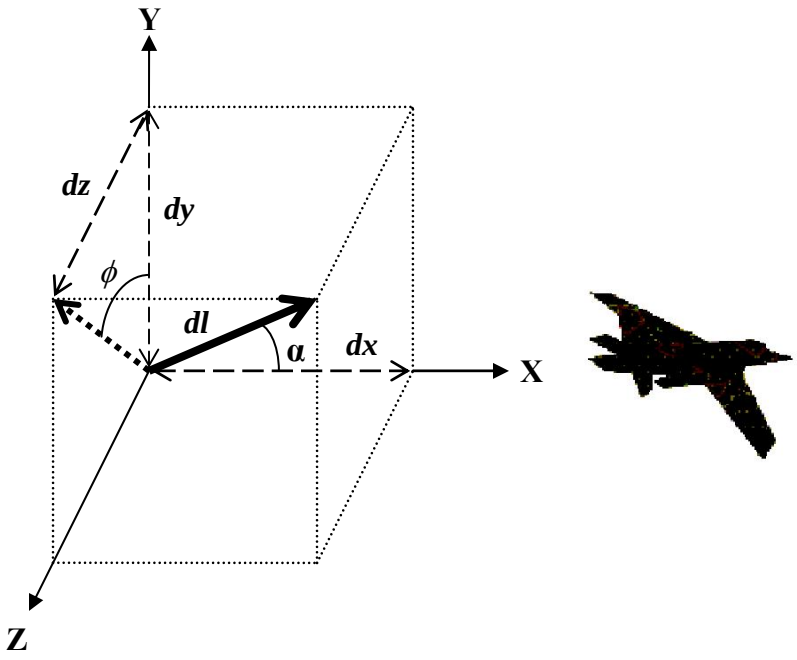

Figure 3. XYZ Coordinate and Polar Towline Reference Frame

Similarly, the rest of the trigonometric functions are

$$\tan\alpha = \frac{\sqrt{\left(\frac{dy}{dl}\right)^2 + \left(\frac{dz}{dl}\right)^2}}{dx/dl} \tag{12}$$

$$\cos\phi = \frac{dy/dl}{\sqrt{\left(\frac{dy}{dl}\right)^2 + \left(\frac{dz}{dl}\right)^2}} \tag{13}$$

$$\sin\phi = \frac{dz/dl}{\sqrt{\left(\frac{dy}{dl}\right)^2 + \left(\frac{dz}{dl}\right)^2}} \tag{14}$$

$$\tan\phi = \frac{dz/dl}{dy/dl} \tag{15}$$

Now that the geometry of the system has been described and all angles are in terms of first order derivatives with respect to *dl*, we can develop the equations of motion. In this case, defining the derivatives with respect to *dl* rather than *dx* is beneficial. The former definition bounds the derivative values between -1 and 1, whereas the latter has unbounded values for the derivatives. For example, for a towline hanging straight down $\frac{dy}{dl} = -1$ but $\frac{dy}{dx} = -\infty$. Avoiding large numbers such as $\pm\infty$ will help decrease computational error.

X-Momentum.

It is well known that the forces of a system in one direction sum to equal the force due to acceleration in that direction. A free body diagram of an elemental length of towline in the xy-plane is provided in Figure 4 to show the forces in the x-direction. The resultant force of the two tensions and the x-component of the drag force must equal the force in the x-direction caused by the acceleration in that direction. Under steady state conditions, this acceleration is zero and the resultant force of the two tensions must equal the x-component of drag. In equation form, this looks like

$$\left(T + \frac{dT}{dl}dl\right)\cos(\alpha + d\alpha) - T\cos\alpha - D_x - D_S = Acc_x \qquad (16)$$

where T is the tension of the towline, D_x is the aforementioned x-component of drag, D_S is the skin friction drag of the towline, and Acc_x is the force due to acceleration in the x-direction.

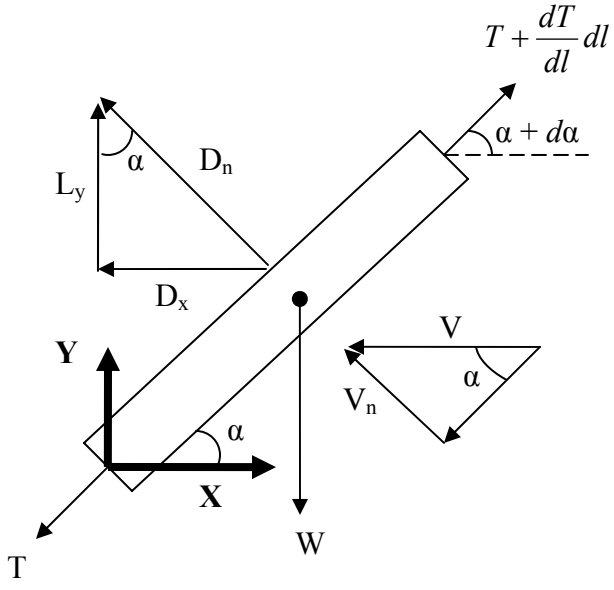

Figure 4. Free Body Diagram of the xy-Plane

Recall from Chapter II the derivation of the component of drag of the towline in the x-direction. Its formula (Barnes and Pothier, 1971:43) is repeated here:

$$D_x = D_n \sin\alpha = \frac{1}{2} C_d \rho_a d_t dl V^2 \sin^3\alpha \tag{4}$$

with C_d representing the coefficient of drag of the towline, ρ_a the density of air, d_t the diameter of the towline, V the freestream velocity of the air, and α the polar angle of the towline with the x-axis. The skin friction drag acts on the towline according to

$$D_S = 0.02 \cdot \rho_a d_t dl V^2 \tag{17}$$

(Hoerner, 1965:2-1). In this work it is assumed that the skin friction drag only acts in the x-direction.

The force due to the acceleration in the x-direction is defined as

$$Acc_x = m_t^{'} dl \frac{d^2 x}{dt^2} \tag{18}$$

where $m_t^{'}$ is the mass per unit length of the towline and the second derivative with respect to time is the acceleration in the x-direction. The mass per unit length of the towline is given by

$$m_t^{'} = \frac{\rho_t \pi d_t^2}{4} \tag{19}$$

where ρ_t is the density of the towline.

The x-momentum equation, Equation 16, can be simplified by using trigonometric identities and other algebraic manipulations to

$$\frac{dT}{dl} - T \tan\alpha \frac{d\alpha}{dl} = \frac{Acc_x + D_x + D_S}{dl \cos\alpha} \tag{20}$$

A new term, $\frac{d\alpha}{dl}$, arises in this equation. Equation 12 can be rewritten to give a definition for α of

$$\alpha = \tan^{-1}\left(\frac{\sqrt{\left(\frac{dy}{dl}\right)^2+\left(\frac{dz}{dl}\right)^2}}{dx/dl}\right) \tag{21}$$

Taking the derivative with respect to *dl* gives

$$\frac{d\alpha}{dl} = \frac{\frac{dx}{dl}\left(\frac{dy}{dl}\cdot\frac{d^2y}{dl^2}+\frac{dz}{dl}\cdot\frac{d^2z}{dl^2}\right)-\frac{d^2x}{dl^2}\left(\left(\frac{dy}{dl}\right)^2+\left(\frac{dz}{dl}\right)^2\right)}{\left(\left(\frac{dx}{dl}\right)^2+\left(\frac{dy}{dl}\right)^2+\left(\frac{dz}{dl}\right)^2\right)\sqrt{\left(\frac{dy}{dl}\right)^2+\left(\frac{dz}{dl}\right)^2}} \tag{22}$$

After making the appropriate substitutions into Equation 20, the x-momentum equation becomes

$$\frac{dT}{dl} - T\cdot\frac{\frac{dx}{dl}\left(\frac{dy}{dl}\cdot\frac{d^2y}{dl^2}+\frac{dz}{dl}\cdot\frac{d^2z}{dl^2}\right)-\frac{d^2x}{dl^2}\left(\left(\frac{dy}{dl}\right)^2+\left(\frac{dz}{dl}\right)^2\right)}{\frac{dx}{dl}\left(\left(\frac{dx}{dl}\right)^2+\left(\frac{dy}{dl}\right)^2+\left(\frac{dz}{dl}\right)^2\right)} = \frac{\left(\frac{\rho_t\pi d_t^2}{4}\cdot\frac{d^2x}{dt^2}+\frac{1}{2}C_d\rho_a d_t V^2\left(\left(\frac{dy}{dx}\right)^2+\left(\frac{dz}{dx}\right)^2\right)^{3/2}+0.02\rho_a d_t V^2\right)}{dx/dl} \tag{23}$$

Y-Momentum.

The same balancing condition of the forces in the x-direction holds for the forces in the y-direction. By examining both Figure 4, the xy-plane, and Figure 5, the yz-plane,

we can identify the forces in the y-direction. Note that in Figure 5 the x-axis is into the page, and also that the elemental length of towline drawn is a projection of the

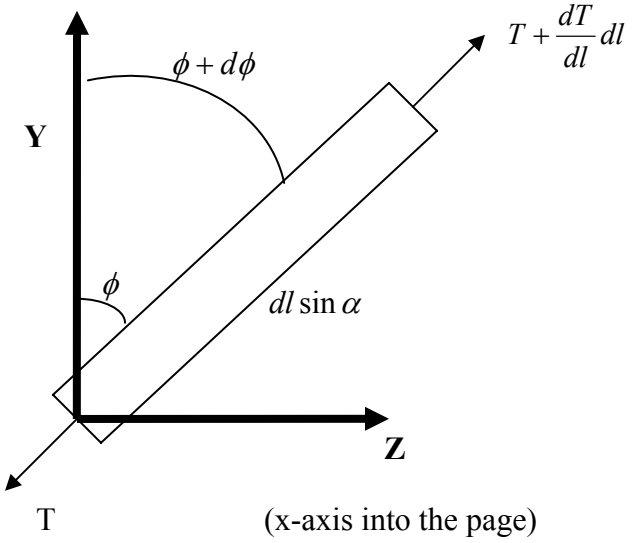

Figure 5. YZ-Plane

towline into the yz-plane and is equal to $dl \sin \alpha$. The resultant of all the forces in the y-direction must equal the force in the y-direction caused by acceleration, given by

$$\left(T + \frac{dT}{dl} dl\right) \sin(\alpha + d\alpha) \cos(\phi + d\phi) - T \sin \alpha \cos \phi - W + L_y = Acc_y \qquad (24)$$

where W is the weight of the towline, L_y is the lift, or component of drag of the towline in the y-direction, and Acc_y is the force due to acceleration in the y-direction. The weight term is described by

$$W = \left(m_t' dl\right) g = \frac{\rho_t \pi d_t^2 dl}{4} g \qquad (25)$$

where g is the acceleration due to gravity. Acc_y is very similar to Acc_x:

$$Acc_y = m_t' dl \frac{d^2 y}{dt^2} \tag{26}$$

The lift term derivation is similar to that of the drag in the x-direction term because both Equation 1 and Equation 2 are used, but in this case D_n is multiplied by $\cos\alpha\cos\phi$:

$$L_y = D_n \cos\alpha\cos\phi = \frac{1}{2} C_d \rho_a d_t dl V^2 \sin^2\alpha\cos\alpha\cos\phi \tag{27}$$

Equation 24 can be simplified by trigonometric identities and algebra to

$$\frac{dT}{dl} + T\left(\cot\alpha\frac{d\alpha}{dl} - \tan\phi\frac{d\phi}{dl}\right) = \frac{Acc_y - L_y + W}{dl\sin\alpha\cos\phi} \tag{28}$$

which contains one new term, $\frac{d\phi}{dl}$. Similar to the derivation of $\frac{d\alpha}{dl}$, the derivation of $\frac{d\phi}{dl}$ involves taking the derivative of Equation 15 solved for ϕ. The result is

$$\frac{d\phi}{dl} = \frac{\frac{dy}{dl}\cdot\frac{d^2 z}{dl^2} - \frac{dz}{dl}\cdot\frac{d^2 y}{dl^2}}{\left(\frac{dy}{dl}\right)^2 + \left(\frac{dz}{dl}\right)^2} \tag{29}$$

When the appropriate substitutions are made, the y-momentum equation becomes very complicated. However, if substitutions are only made for the force terms on the right hand side of the equation, it remains readable:

$$\frac{dT}{dl} + T\left(\cot\alpha\frac{d\alpha}{dl} - \tan\phi\frac{d\phi}{dl}\right) = \tag{30}$$

$$\frac{\frac{\rho_t \pi d_t^2}{4}\frac{d^2 y}{dt^2} - \frac{1}{2} C_d \rho_a d_t V^2 \sin^2\alpha\cos\alpha\cos\phi + \frac{\rho_t \pi d_t^2}{4} g}{\sin\alpha\cos\phi}$$

The reader should note that additional substitutions could have been made for the trigonometric functions and the $\frac{d\alpha}{dl}$ and $\frac{d\phi}{dl}$ terms.

Z-Momentum.

Deriving the z-momentum equation is a matter of repeating the process used for the x and y-momentum equations. The forces in the z-direction are illustrated in Figure 5 and Figure 6. In Figure 6 the y-axis is out of the page.

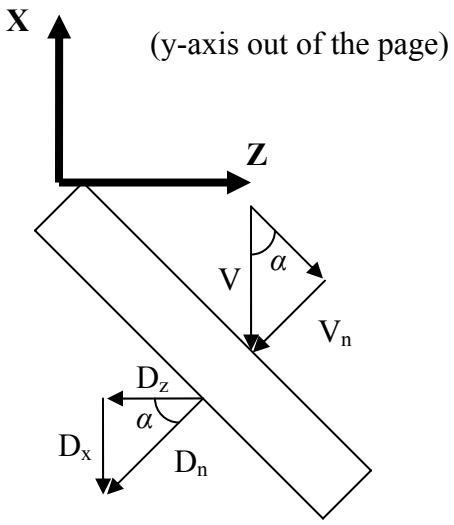

Figure 6. XZ-Plane

As before, the sum of the forces equals the force due to acceleration:

$$\left(T+\frac{dT}{dl}dl\right)\sin(\alpha+d\alpha)\sin(\phi+d\phi)-T\sin\alpha\sin\phi-D_z=Acc_z \qquad (31)$$

where D_z is the component of drag in the z-direction and Acc_z is the force due to acceleration in the z-direction. The derivation of the formula for D_z is similar to the derivation of lift, with D_n multiplied by $\cos\alpha\sin\phi$:

$$D_z = D_n \cos\alpha \sin\phi = \frac{1}{2} C_d \rho_a d_t dl V^2 \sin^2\alpha \cos\alpha \sin\phi \tag{32}$$

Acc_z looks like Acc_x and Acc_y, only with z as the variable in the second order time derivative:

$$Acc_z = m_t' dl \frac{d^2 z}{dt^2} \tag{33}$$

Using the same trigonometric identities and algebra as with the other two derivations, the z-momentum equation can be expressed as

$$\frac{dT}{dl} + T\left(\cot\alpha \frac{d\alpha}{dl} + \cot\phi \frac{d\phi}{dl}\right) = \frac{Acc_z + D_x}{dl \sin\alpha \sin\phi} \tag{34}$$

Similar to the y-momentum equation, making all the appropriate substitutions into Equation 34 gives a complex, confusing equation. For the convenience of the reader only the force terms will be substituted in on the right hand side:

$$\frac{dT}{dl} + T\left(\cot\ \alpha\ \frac{d\alpha}{dl} + \cot\ \phi\ \frac{d\phi}{dl}\right) = \frac{\frac{\rho_t \pi d_t^2}{4} \frac{d^2 z}{dt^2} + \frac{1}{2} C_d \rho_a d_t V^2 \sin^2\alpha \cos\alpha \sin\phi}{\sin\alpha \sin\phi} \tag{35}$$

Nondimensionalization

The equations can be nondimensionalized to gain insight as to which system parameters affect the towline shape and position. This will also determine the manner in which they have an effect. To make the variables dimensionless, the following substitutions can be made:

$$dl^* = \frac{dl}{L} \qquad dx^* = \frac{dx}{L} \qquad dy^* = \frac{dy}{L} \qquad dz^* = \frac{dz}{L}$$

$$d^2x^* = \frac{d^2x}{L} \qquad d^2y^* = \frac{d^2y}{L} \qquad d^2z^* = \frac{d^2z}{L}$$

$$\left(dl^*\right)^2 = \frac{dl^2}{L^2} \qquad \left(dt^*\right)^2 = \frac{dt^2}{\tau_c^2}$$

$$T^* = \frac{T}{T_0} \qquad dT^* = \frac{dT}{T_0}$$

where L is the length of the towline, τ_c is a characteristic time of the system to be determined later, and T_0 is a characteristic tension of the system, also to be defined later. In nondimensionalizing, the trigonometric functions such as $\cos\alpha$, $\sin\alpha$, etc. remain unchanged because they are nondimensional by definition. However, a $\frac{1}{L}$ is factored out of both $\frac{d\alpha}{dl}$ and $\frac{d\phi}{dl}$ when the substitutions are completed. As an example, the x-momentum equation would become

$$\frac{T_0}{L}\frac{dT^*}{dl^*} - T_0 T^* \tan\alpha \frac{1}{L}\left(\frac{d\alpha}{dl}\right)^* =$$

$$\frac{\frac{\rho_t \pi d_t^2}{4}\cdot\frac{L}{\tau_c^2}\cdot\frac{d^2x^*}{\left(dt^*\right)^2} + \frac{1}{2}C_d\rho_a d_t V^2 \sin^3\alpha + 0.02\,\rho_a d_t V^2}{\cos\alpha} \tag{36}$$

Using algebra with the desire to have C_d alone in front of the sine-cubed term, the equation can be rewritten as

$$\frac{2T_0}{L\rho_a d_t V^2}\frac{dT^*}{dl^*} - \frac{2T_0}{L\rho_a d_t V^2}T^* \tan\alpha\left(\frac{d\alpha}{dl}\right)^* =$$

$$\frac{\frac{\rho_t \pi d_t L}{2\rho_a V^2 \tau_c^2}\cdot\frac{d^2x^*}{\left(dt^*\right)^2} + C_d \sin^3\alpha + 0.04}{\cos\alpha} \tag{37}$$

Similarly, the y-momentum and z-momentum equations can be expressed as

$$\frac{2T_0}{L\rho_a d_t V^2}\frac{dT^*}{dl^*} + \frac{2T_0}{L\rho_a d_t V^2}T^*\left(\cot\alpha\left(\frac{d\alpha}{dl}\right)^* - \tan\phi\left(\frac{d\phi}{dl}\right)^*\right) =$$

$$\frac{\frac{\rho_t \pi d_t L}{2\rho_a V^2 \tau_c^2}\cdot\frac{d^2y^*}{\left(dt^*\right)^2} - C_d \sin^2\alpha\cos\alpha\cos\phi + \frac{\rho_t \pi d_t}{2\rho_a V^2}g}{\sin\alpha\cos\phi} \tag{38}$$

and

$$\frac{2T_0}{L\rho_a d_t V^2}\frac{dT^*}{dl^*} + \frac{2T_0}{L\rho_a d_t V^2}T^*\left(\cot\alpha\left(\frac{d\alpha}{dl}\right)^* + \cot\phi\left(\frac{d\phi}{dl}\right)^*\right) =$$

$$\frac{\frac{\rho_t \pi d_t L}{2\rho_a V^2 \tau_c^2}\cdot\frac{d^2z^*}{\left(dt^*\right)^2} + C_d \sin^2\alpha\cos\alpha\sin\phi}{\sin\alpha\sin\phi} \tag{39}$$

respectively.

Numerical Integration

Since the towline shape is the interest of this work, we need to obtain from the nondimensional differential equations the (x,y,z) positions along the length of the towline. This can be done using numerical integration. The solver will need a system of differential equations to integrate and a set of conditions applicable to the system.

The system of differential equations needed to understand the towed decoy system consists of seven equations, four first order differential equations and three second order differential equations. These seven equations are equations for $\frac{dx}{dl}$, $\frac{dy}{dl}$, $\frac{dz}{dl}$, $\frac{dT}{dl}$, $\frac{d^2x}{dl^2}$, $\frac{d^2y}{dl^2}$, and $\frac{d^2z}{dl^2}$. The first three are Equations 5-7 divided by *dl* on both sides. The last four can be solved for using the three momentum equations described earlier and an additional fourth equation. This fourth equation comes from dividing Equation 8 by *dl* on both sides, and then taking the derivative with respect to *dl*:

$$0 = \frac{dx}{dl}\cdot\frac{d^2x}{dl^2} + \frac{dy}{dl}\cdot\frac{d^2y}{dl^2} + \frac{dz}{dl}\cdot\frac{d^2z}{dl^2} \tag{40}$$

Mathematica® was used to solve the four equations (Equations 37-40) and four unknowns ($\frac{dT}{dl}$, $\frac{d^2x}{dl^2}$, $\frac{d^2y}{dl^2}$, and $\frac{d^2z}{dl^2}$) system and gave the following as output:

$$\frac{dT^*}{dl^*}=\frac{\left(\begin{array}{c}0.04\dfrac{dx^*}{dl^*}+2C_d\dfrac{dx^*}{dl^*}\left(\dfrac{dz^*}{dl^*}\right)^2\sqrt{\left(\dfrac{dy^*}{dl^*}\right)^2+\left(\dfrac{dz^*}{dl^*}\right)^2}+\dfrac{\rho_t\pi d_t}{2\rho_a V^2}g\dfrac{dy^*}{dl^*}\\ +\dfrac{\rho_t\pi d_t L}{2\rho_a V^2\tau_c^2}\left(\dfrac{d^2x^*}{\left(dt^*\right)^2}\dfrac{dx^*}{dl^*}+\dfrac{d^2y^*}{\left(dt^*\right)^2}\dfrac{dy^*}{dl^*}+\dfrac{d^2z^*}{\left(dt^*\right)^2}\dfrac{dz^*}{dl^*}\right)\end{array}\right)}{\dfrac{2T_0}{L\rho_a d_t V^2}\left(\left(\dfrac{dx^*}{dl^*}\right)^2+\left(\dfrac{dy^*}{dl^*}\right)^2+\left(\dfrac{dz^*}{dl^*}\right)^2\right)} \tag{41}$$

$$\frac{d^2x^*}{\left(dl^*\right)^2}=\frac{\left(\begin{array}{c}0.04\left(\left(\dfrac{dy^*}{dl^*}\right)^2+\left(\dfrac{dz^*}{dl^*}\right)^2\right)-\dfrac{\rho_t\pi d_t}{2\rho_a V^2}g\dfrac{dx^*}{dl^*}\dfrac{dy^*}{dl^*}\\ +C_d\sqrt{\left(\dfrac{dy^*}{dl^*}\right)^2+\left(\dfrac{dz^*}{dl^*}\right)^2}\left[\left(\dfrac{dx^*}{dl^*}\right)^2\left(\left(\dfrac{dy^*}{dl^*}\right)^2-\left(\dfrac{dz^*}{dl^*}\right)^2\right)+\left(\left(\dfrac{dy^*}{dl^*}\right)^2+\left(\dfrac{dz^*}{dl^*}\right)^2\right)^2\right]\\ +\dfrac{\rho_t\pi d_t L}{2\rho_a V^2\tau_c^2}\left(\dfrac{d^2x^*}{\left(dt^*\right)^2}\left(\left(\dfrac{dy^*}{dl^*}\right)^2+\left(\dfrac{dz^*}{dl^*}\right)^2\right)-\dfrac{d^2y^*}{\left(dt^*\right)^2}\dfrac{dx^*}{dl^*}\dfrac{dy^*}{dl^*}-\dfrac{d^2z^*}{\left(dt^*\right)^2}\dfrac{dx^*}{dl^*}\dfrac{dz^*}{dl^*}\right)\end{array}\right)}{T^*\dfrac{2T_0}{L\rho_a d_t V^2}\left(\left(\dfrac{dx^*}{dl^*}\right)^2+\left(\dfrac{dy^*}{dl^*}\right)^2+\left(\dfrac{dz^*}{dl^*}\right)^2\right)} \tag{42}$$

$$\frac{d^2y^*}{\left(dl^*\right)^2}=\frac{\left(\begin{array}{c}-0.04\dfrac{dx^*}{dl^*}\dfrac{dy^*}{dl^*}+\dfrac{\rho_t\pi d_t}{2\rho_a V^2}g\left(\left(\dfrac{dx^*}{dl^*}\right)^2+\left(\dfrac{dz^*}{dl^*}\right)^2\right)\\ -C_d\dfrac{dx^*}{dl^*}\dfrac{dy^*}{dl^*}\sqrt{\left(\dfrac{dy^*}{dl^*}\right)^2+\left(\dfrac{dz^*}{dl^*}\right)^2}\left(\left(\dfrac{dx^*}{dl^*}\right)^2+\left(\dfrac{dy^*}{dl^*}\right)^2+3\left(\dfrac{dz^*}{dl^*}\right)^2\right)\\ +\dfrac{\rho_t\pi d_t L}{2\rho_a V^2\tau_c^2}\left(-\dfrac{d^2x^*}{\left(dt^*\right)^2}\dfrac{dx^*}{dl^*}\dfrac{dy^*}{dl^*}+\dfrac{d^2y^*}{\left(dt^*\right)^2}\left(\left(\dfrac{dx^*}{dl^*}\right)^2+\left(\dfrac{dz^*}{dl^*}\right)^2\right)-\dfrac{d^2z^*}{\left(dt^*\right)^2}\dfrac{dy^*}{dl^*}\dfrac{dz^*}{dl^*}\right)\end{array}\right)}{T^*\dfrac{2T_0}{L\rho_a d_t V^2}\left(\left(\dfrac{dx^*}{dl^*}\right)^2+\left(\dfrac{dy^*}{dl^*}\right)^2+\left(\dfrac{dz^*}{dl^*}\right)^2\right)}- \tag{43}$$

$$\frac{d^2z^*}{\left(dl^*\right)^2}=\frac{\left(\begin{array}{c}-0.04\dfrac{dx^*}{dl^*}\dfrac{dz^*}{dl^*}-\dfrac{\rho_t\pi d_t}{2\rho_a V^2}g\dfrac{dy^*}{dl^*}\dfrac{dz^*}{dl^*}\\ +C_d\dfrac{dx^*}{dl^*}\dfrac{dz^*}{dl^*}\sqrt{\left(\dfrac{dy^*}{dl^*}\right)^2+\left(\dfrac{dz^*}{dl^*}\right)^2}\left(\left(\dfrac{dx^*}{dl^*}\right)^2+\left(\dfrac{dy^*}{dl^*}\right)^2-\left(\dfrac{dz^*}{dl^*}\right)^2\right)\\ +\dfrac{\rho_t\pi d_t L}{2\rho_a V^2\tau_c^2}\left(-\dfrac{d^2x^*}{\left(dt^*\right)^2}\dfrac{dx^*}{dl^*}\dfrac{dz^*}{dl^*}-\dfrac{d^2y^*}{\left(dt^*\right)^2}\dfrac{dy^*}{dl^*}\dfrac{dz^*}{dl^*}+\dfrac{d^2z^*}{\left(dt^*\right)^2}\left(\left(\dfrac{dx^*}{dl^*}\right)^2+\left(\dfrac{dy^*}{dl^*}\right)^2\right)\right)\end{array}\right)}{T^*\dfrac{2T_0}{L\rho_a d_t V^2}\left(\left(\dfrac{dx^*}{dl^*}\right)^2+\left(\dfrac{dy^*}{dl^*}\right)^2+\left(\dfrac{dz^*}{dl^*}\right)^2\right)} \tag{44}$$

The seven equations have now been identified (Equations 5-7 and 41-44). They can be implemented into a numerical integration routine as follows:

$$f(1)=x=\int\frac{dx}{dl}dl=\int f(5)\cdot dl \tag{45}$$

$$f(2)=y=\int\frac{dy}{dl}dl=\int f(6)\cdot dl \tag{46}$$

$$f(3)=z=\int\frac{dz}{dl}dl=\int f(7)\cdot dl \tag{47}$$

$$f(4)=T=\int\frac{dT}{dl}dl \tag{48}$$

$$f(5)=\frac{dx}{dl}=\int\frac{d^2x}{dl^2}dl \tag{49}$$

$$f(6)=\frac{dy}{dl}=\int\frac{d^2y}{dl^2}dl \tag{50}$$

$$f(7)=\frac{dz}{dl}=\int\frac{d^2z}{dl^2}dl \tag{51}$$

where f is an arbitrary vector containing the equations to be integrated.

The decoy end of the towline is chosen as the starting point for the numerical integration along the towline in the steady state case because the initial conditions are known at that end. The initial condition for x, y, and z can be arbitrarily assigned as 0.

$$x_i = 0 \qquad y_i = 0 \qquad z_i = 0 \tag{52}$$

The initial condition for T is the resultant force of the decoy forces, or

$$T_i = \sqrt{(D_{Dx})^2 + (L_D - W_D)^2 + (D_{Dz})^2} \tag{53}$$

where D_{Dx} is the component of drag of the decoy in the x-direction, L_D is the lift generated by the decoy, W_D is the weight of the decoy, and D_{Dz} is the component of drag of the decoy in the z-direction. The x-component of drag is given by

$$D_{Dx} = \frac{1}{2} C_{dD} \rho_a \pi \frac{d_d^2}{4} V_{rel} V_x \tag{54}$$

where C_{dD} is the coefficient of drag of the decoy, d_D is the diameter of the decoy, V_{rel} is the relative velocity, and V_x is the component of velocity in the x-direction. Similarly, L_D and D_{Dz} are defined as

$$L_D = \frac{1}{2} C_{dD} \rho_a \pi \frac{d_d^2}{4} V_{rel} V_y \tag{55}$$

and

$$D_{Dz} = \frac{1}{2} C_{dD} \rho_a \pi \frac{d_d^2}{4} V_{rel} V_z \tag{56}$$

respectively, with V_y representing the y-component of velocity and V_z the z-component of velocity. The weight of the decoy can be expressed as

$$W_D = m_D g \tag{57}$$

where m_D is the mass of the decoy. The initial value for the angle α is

$$\alpha_i = \frac{\sqrt{(W_D - L_D)^2 + (D_{Dz})^2}}{D_{Dx}} \tag{58}$$

and the initial value for the angle ϕ is

$$\phi_i = \tan^{-1}\left(\frac{D_{Dz}}{W_D - L_D}\right) \tag{59}$$

This determines the remaining initial values needed:

$$\left(\frac{dx}{dl}\right)_i = \cos\alpha_i \tag{60}$$

$$\left(\frac{dy}{dl}\right)_i = \sin\alpha_i \cos\phi_i \tag{61}$$

$$\left(\frac{dz}{dl}\right)_i = \sin\alpha_i \sin\phi_i \tag{62}$$

Now the equations to be integrated, Equations 45-51, and the initial values, Equations 52, 53 and 60-62, can be given to a numerical ordinary differential equation solver. The solver used in this work is *ode45* of MATLAB®, which is a fourth order Runge-Kutta routine. The solver starts at the decoy end of the towline and integrates along the towline at steps of various lengths, producing a vector *p* and an array of vectors *q* as output. The variables *p* and *q* were chosen arbitrarily to avoid having duplicate variables in the text. The vector *p* contains all the steps, or values of the independent variable *dl*, of integration. The array *q* contains vectors of the values of the integrals of the equations (Equations 45-51) at each independent variable step. As an example, the first vector in the array *q* gives the values of the integral of Equation 45, which are the values of the x-position corresponding to the values of *dl* in the vector *p*. The second vector in *q* would be the y-position values, the third the z-position, and so on. The last

information the solver needs is the interval of values of the independent variable to integrate over. Since we are integrating with respect to the nondimensional $\frac{dl}{L}$, the interval is 0 to 1, representing one end of the towline to the other.

Assumptions

The procedure described thus far in this chapter relies heavily upon theory, and can be applied to almost every case, with the exception of the generation of initial values for the ordinary differential equations. The steady state case is one in which all initial values are known – an initial value problem. Not all the initial values will be known in every case, and in those instances this will be a boundary value problem with known boundary conditions at both ends instead.

In turns out that some assumptions can be made for the steady state case that reduces the complexity of the problem. One is that the derivatives with respect to time equal zero and those terms can be removed from the equations. Another assumption made in this work is that the velocity of the air acts along the x-axis only. With both V_y and V_z equal to 0, there is no component of drag in the z-direction for neither the towline nor the decoy, and no lift is generated by the decoy. This essentially constrains the problem to the xy-plane. The z-coordinate will be 0 at every position along the towline in this steady state case. This leads to a simplification of the differential equations:

$$\frac{dT^*}{dl^*} = \frac{0.04\frac{dx^*}{dl^*} + 2C_d\frac{dx^*}{dl^*}\left(\frac{dz^*}{dl^*}\right)^2\sqrt{\left(\frac{dy^*}{dl^*}\right)^2 + \left(\frac{dz^*}{dl^*}\right)^2} + \frac{\rho_t \pi d_t}{2\rho_a V^2} g\frac{dy^*}{dl^*}}{\frac{2T_0}{L\rho_a d_t V^2}\left(\left(\frac{dx^*}{dl^*}\right)^2 + \left(\frac{dy^*}{dl^*}\right)^2 + \left(\frac{dz^*}{dl^*}\right)^2\right)} \qquad (63)$$

$$\frac{d^2x^*}{\left(dl^*\right)^2}=\frac{\left(\begin{array}{c}0.04\left(\left(\frac{dy^*}{dl^*}\right)^2+\left(\frac{dz^*}{dl^*}\right)^2\right)-\frac{\rho_t\pi d_t}{2\rho_a V^2}g\frac{dx^*}{dl^*}\frac{dy^*}{dl^*}\\ +C_d\sqrt{\left(\frac{dy^*}{dl^*}\right)^2+\left(\frac{dz^*}{dl^*}\right)^2}\left(\left(\frac{dx^*}{dl^*}\right)^2\left(\left(\frac{dy^*}{dl^*}\right)^2-\left(\frac{dz^*}{dl^*}\right)^2\right)+\left(\left(\frac{dy^*}{dl^*}\right)^2+\left(\frac{dz^*}{dl^*}\right)^2\right)^2\right)\end{array}\right)}{T^*\frac{2T_0}{L\rho_a d_t V^2}\left(\left(\frac{dx^*}{dl^*}\right)^2+\left(\frac{dy^*}{dl^*}\right)^2+\left(\frac{dz^*}{dl^*}\right)^2\right)} \tag{64}$$

$$\frac{d^2y^*}{\left(dl^*\right)^2}=\frac{\left(\begin{array}{c}-0.04\frac{dx^*}{dl^*}\frac{dy^*}{dl^*}+\frac{\rho_t\pi d_t}{2\rho_a V^2}g\left(\left(\frac{dx^*}{dl^*}\right)^2+\left(\frac{dz^*}{dl^*}\right)^2\right)\\ -C_d\sqrt{\left(\frac{dy^*}{dl^*}\right)^2+\left(\frac{dz^*}{dl^*}\right)^2}\frac{dx^*}{dl^*}\frac{dy^*}{dl^*}\left(\left(\frac{dx^*}{dl^*}\right)^2+\left(\frac{dy^*}{dl^*}\right)^2+3\left(\frac{dz^*}{dl^*}\right)^2\right)\end{array}\right)}{T^*\frac{2T_0}{L\rho_a d_t V^2}\left(\left(\frac{dx^*}{dl^*}\right)^2+\left(\frac{dy^*}{dl^*}\right)^2+\left(\frac{dz^*}{dl^*}\right)^2\right)} \tag{65}$$

$$\frac{d^2z^*}{\left(dl^*\right)^2}=\frac{-\frac{dz^*}{dl^*}\left(\begin{array}{c}0.04\frac{dx^*}{dl^*}+\frac{\rho_t\pi d_t}{2\rho_a V^2}g\frac{dy^*}{dl^*}\\ -C_d\sqrt{\left(\frac{dy^*}{dl^*}\right)^2+\left(\frac{dz^*}{dl^*}\right)^2}\frac{dx^*}{dl^*}\left(\left(\frac{dx^*}{dl^*}\right)^2+\left(\frac{dy^*}{dl^*}\right)^2-\left(\frac{dz^*}{dl^*}\right)^2\right)\end{array}\right)}{T^*\frac{2T_0}{L\rho_a d_t V^2}\left(\left(\frac{dx^*}{dl^*}\right)^2+\left(\frac{dy^*}{dl^*}\right)^2+\left(\frac{dz^*}{dl^*}\right)^2\right)} \tag{66}$$

The MATLAB® code written to utilize *ode45* in solving these differential equations for this research is included in Appendix A.

IV: Results and Discussion

The derivation of the equations of motion, followed by nondimensionalizing those equations, led to the identification of parameter groups that play a role in determining the towline shape and position. Numerical integration can then be used to generate the shape of the towline for a given combination of parameter group values. The shapes can be compared to ascertain a relation between the parameter groups and the towline shape.

Parameter Groups

The important parameter groups in the towed decoy system can be identified by examining Equations 37-39 and 58. In these equations, four different nondimensional groups are present. One of them is

$$\frac{2T_0}{L\rho_a d_t V^2}$$

and will be referred to as the *tension group*. A second group that emerged is

$$\frac{\rho_t \pi d_t L}{2\rho_a V^2 \tau_c^2}$$

and this group will be called the *acceleration group*. This group can lead to the definition of the characteristic time of the towline:

$$\tau_c = \sqrt{\frac{\rho_t \pi d_t L}{2\rho_a V^2}} \tag{67}$$

This characteristic time describes the length of time it takes for the towline to respond to an impulse. A third nondimensional group, which will be known as the *body force group*, is

$$\frac{\rho_t \pi d_t}{2 \rho_a V^2} g$$

Finally, the fourth group is

$$\frac{\sqrt{(W_D - L_D)^2 + (D_{Dz})^2}}{D_{Dx}}$$

and will be referred to as the *decoy weight to drag ratio.* Under the assumptions made in this work, the *decoy weight to drag ratio* reduces to

$$\frac{W_D}{D_{Dx}}$$

The assumptions described in the previous chapter also eliminate the need to incorporate the *acceleration group* because it is always multiplied by a time derivative. The time derivatives are 0 in this research.

The description that T_0 is a characteristic tension of the system was given previously, but no formal mathematical formula was offered. If we choose to define T_0 as the weight of the entire towline, the solution space can be reduced by one more group. Substituting

$$T_0 = \frac{\rho_t \pi d_t^2 L}{4} g \tag{68}$$

in for T_0 in the *tension group* reveals

$$\frac{2T_0}{L \rho_a d_t V^2} = \frac{\rho_t \pi d_t}{2 \rho_a V^2} g \tag{69}$$

which is exactly equal to the *body force group*. In other words, only the *body force group* and the *decoy weight to drag ratio* affect the towline shape in the steady state condition. Likewise, the parameters making up these two groups are the only parameters that affect the steady state system.

To understand the effect that each group has on the towline shape, a range of values for each of the parameters making up the groups is given in Table 1, followed by the resulting range of the *body force group* and the *decoy weight to drag ratio*. A large range was chosen for each value in an attempt to incorporate all values the system might encounter. The range of the *decoy weight to drag ratio* is from 1.6E-4 to 3672. The *body force group* has a range from 3.0E-5 to 15. These ranges can be used to generate plots of towline shapes.

Table 1 Parametric Study

Parameter	Low Value	High Value	Units
ρ_t	500	2000	kg/m^3
d_t	0.005	0.05	m
g	9.8	9.8	m/s^2
ρ_a	0.12081	1.2256	kg/m^3
V	30	1000	m/s
m_D	2	20	kg
C_{dD}	0.5	2	unitless
d_D	0.05	0.35	m
Body Force Group	3.0E-5	15	unitless
Decoy Weight to Drag Ratio	1.6E-4	3672	unitless

A typical value for the *body force group* is 0.071, resulting from a towline density of 1200 kg/m^3, a towline diameter of 1 cm, an air density of 0.041351 kg/m^3, and a velocity of 250 m/s. A typical *decoy weight to drag ratio*, calculated with a decoy mass of 5 kg, decoy coefficient of drag of 1, and a decoy diameter of 10 cm at the same air density and velocity as the first group, is 4.83.

Towline Shapes

The code in Appendix A creates a plot of the xy-plane when the numerical integration has completed. A typical plot is shown in Figure 7. In this figure, the *decoy weight to drag ratio* is 0.2, and the range of the *body force group* is represented by the multiple towline shapes plotted on the same graph. The value of the *body force group* is printed next to the corresponding towline shape. The decoy location is where all the shapes meet in the lower left corner, and the aircraft would be at the opposite end of a particular towline shape. In other words, the decoy location is constant at (0, 0) whereas the aircraft location varies according to the *body force group* value. In Figure 7 the towlines with values for the *body force group* greater than 0.1 exhibit a concave up shape, or positive curvature, while the values of 0.1 and less display a concave down shape, or negative curvature.

Figure 8 shows the towline shapes when the *decoy weight to drag ratio* is at its extreme low value of 1.6E-4. When the ratio is at its lowest value, the fanning out of the end of the towlines is less pronounced than in Figure 7. The shapes are closer together,

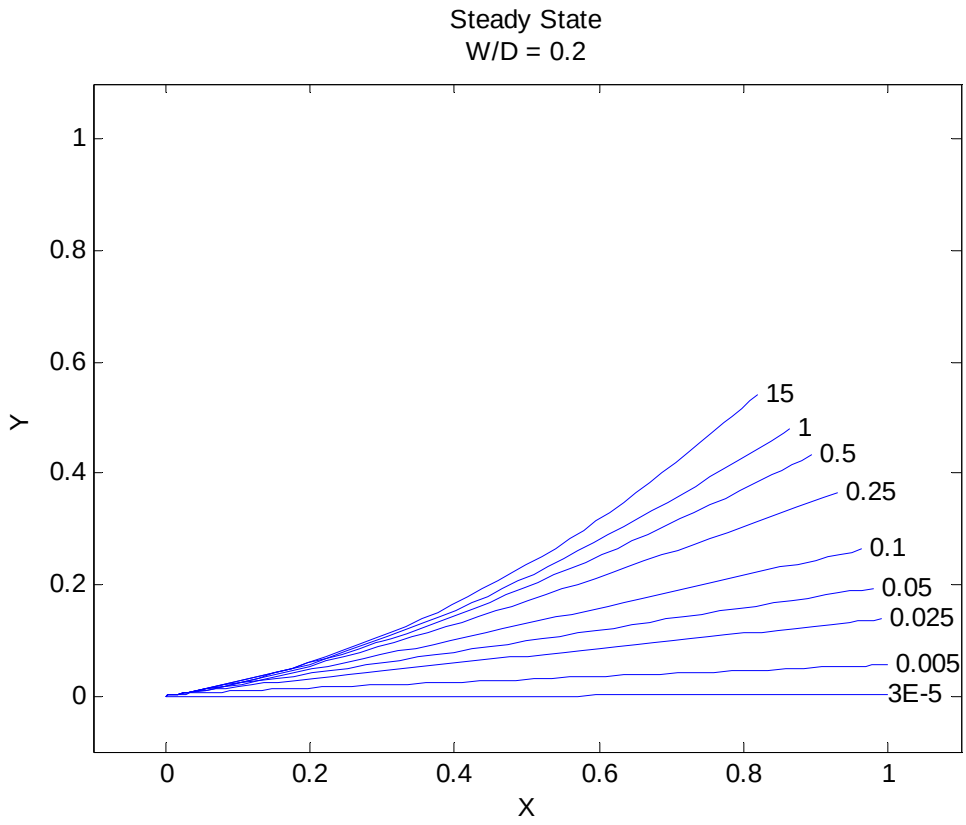

Figure 7. Towline Shapes with Decoy Drag to Weight Ratio = 0.2

with the positive curvature property being extended to nearly all the towline shapes, with the exception of the one with the *body force group* equal to 3.0E-5 which again displays a linear shape straight out the back of the aircraft. Figure 9 illustrates the towline shapes when the ratio is increased to 0.05. It shows less fanning at the end of the towlines than Figure 7 but more than Figure 8. The curvature is also somewhere in the middle of the curvature exhibited in Figure 7 and Figure 8 – there are more towlines with positive curvature than Figure 7 with the higher *decoy weight to drag ratio*, but less towlines with the same shape property than in Figure 8 with the lower *decoy weight to drag ratio*.

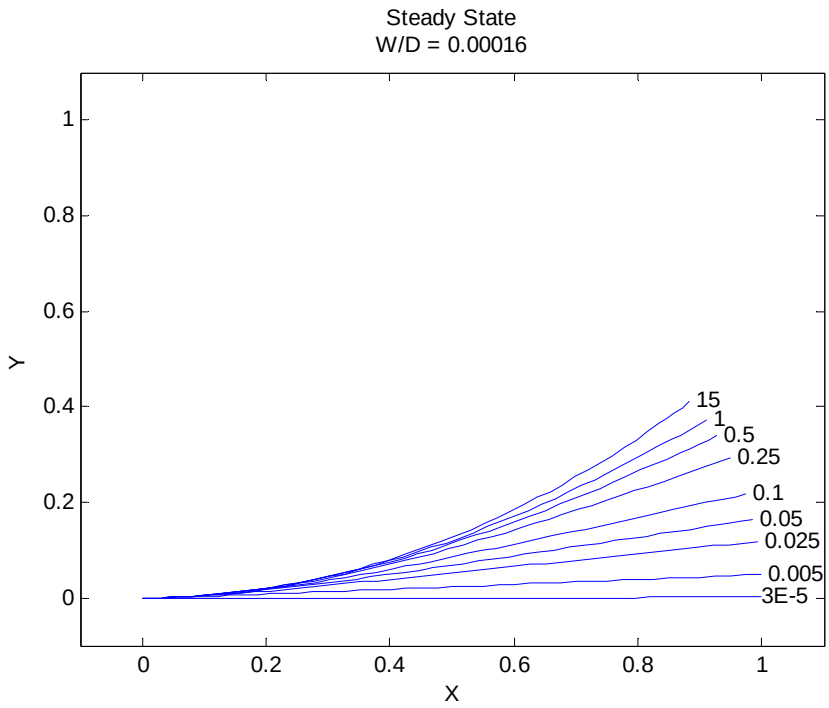

Figure 8. Towline Shapes with Decoy Drag to Weight Ratio = 1.6E-4

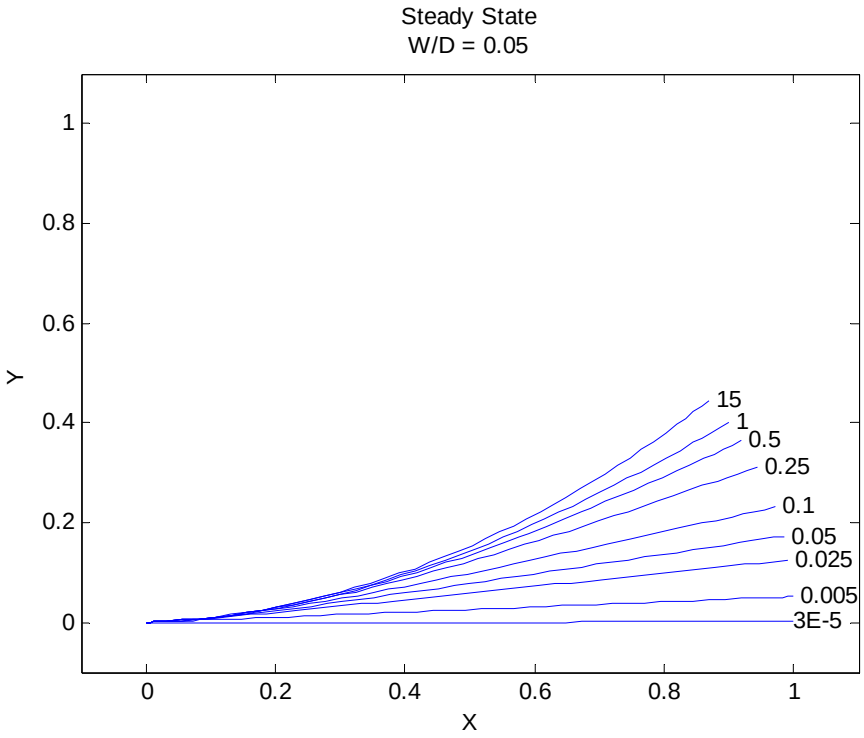

Figure 9. Towline Shapes with Decoy Drag to Weight Ratio = 0.05

The effect of increasing the *decoy weight to drag ratio* by a factor of 10 to 0.5 is shown in Figure 10. The spreading out of the towlines is the greatest out of the results so far at this higher ratio. The number of shapes that have positive curvature is also the lowest so far, with only the towlines with *body force group* values of 0.5 or greater displaying the trait. Figure 11 illustrates towline shapes when the *decoy drag to weight ratio* is doubled to 1. The same trends continue with additional spreading out of the towline shapes and fewer shapes with positive curvature. The towlines with the lower values for the *body force group* exhibit a more pronounced negative curvature attribute while only the highest values display positive curvature. The *decoy weight to drag ratio* is increased to 5 in Figure 12 and the same trends hold. Here the negative curvature trait

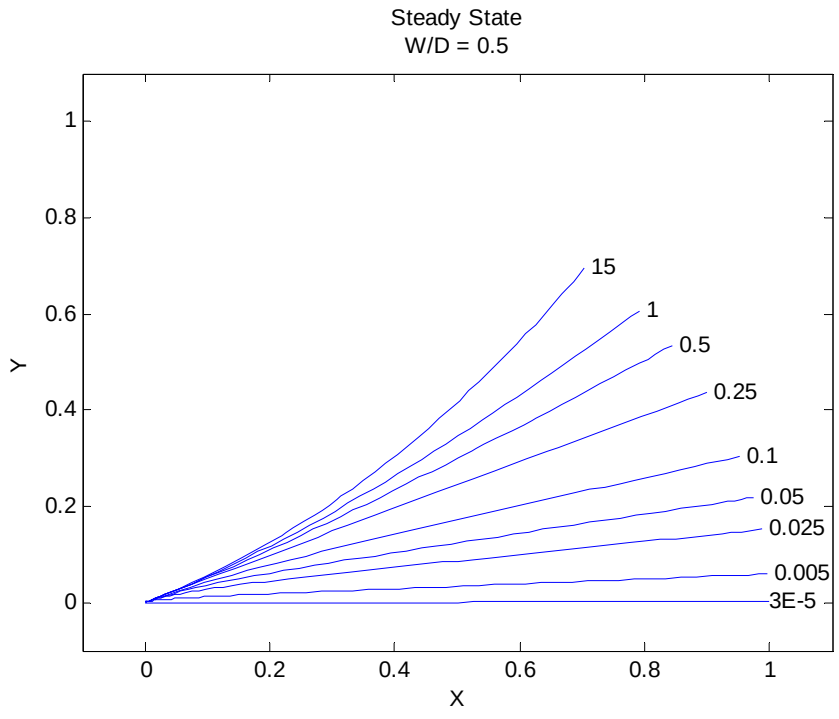

Figure 10. Towline Shapes with Decoy Drag to Weight Ratio = 0.5

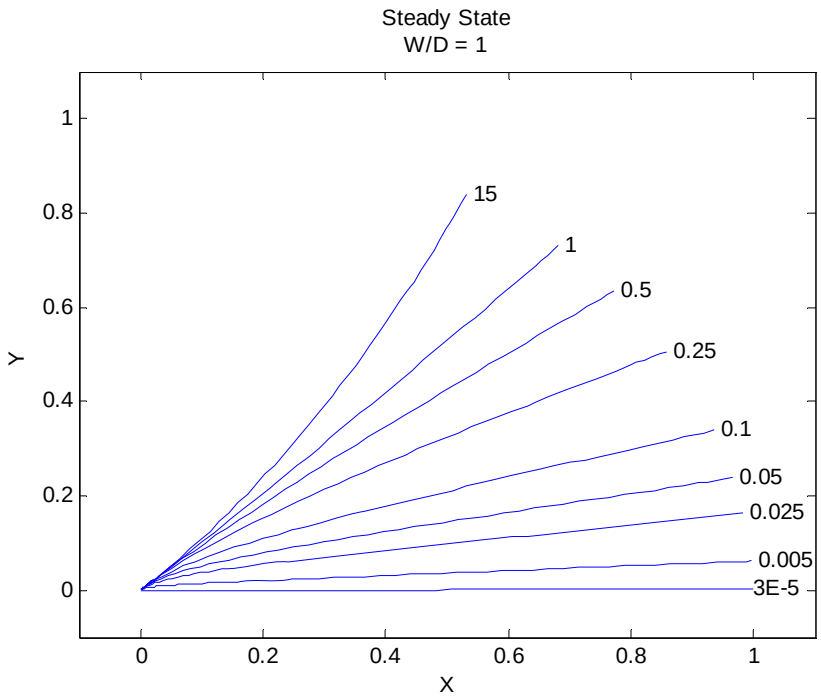

Figure 11. Towline Shapes with Decoy Drag to Weight Ratio = 1

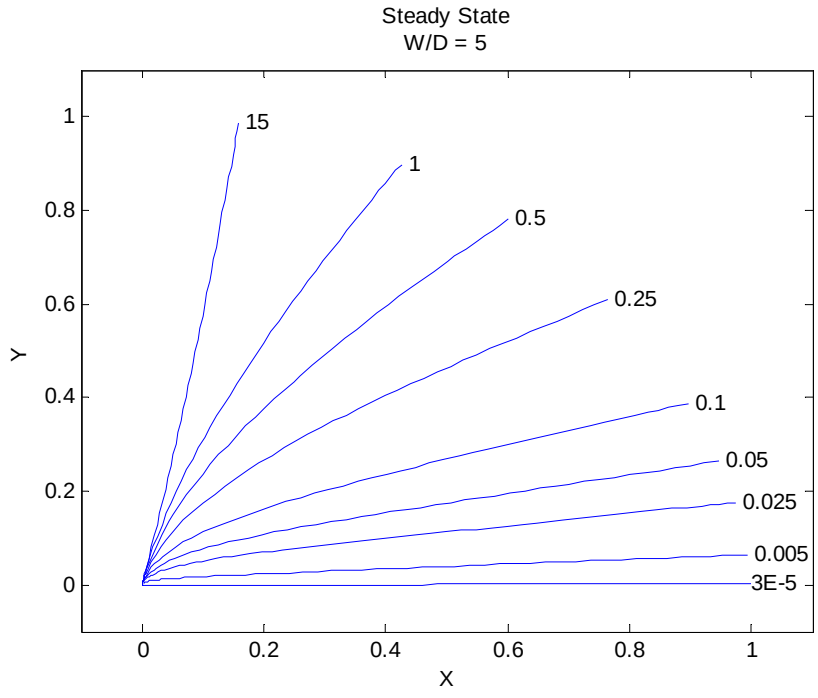

Figure 12. Towline Shapes with Decoy Drag to Weight Ratio = 5

of the shapes is clearly visible, other than in the shape for the towline with a *body force group* value of 15.

The last four figures provided illustrate towline shapes at the high end of the range for the *decoy weight to drag ratio*. Figure 13, Figure 14, Figure 15, and Figure 16 display towline shapes resulting from *decoy weight to drag ratio* values of 10, 100, 1000, and 3672 respectively. The towline shapes are very similar for all four plots. The range of values for the *body force group* completely spreads out the towline shapes, with the lowest value exhibiting a horizontal shape and the highest value demonstrating a nearly vertical shape in all four plots. Every towline shape has negative curvature in the last three plots, and only one has positive curvature in Figure 13. A small amount of spreading out can be seen when moving from Figure 13 to Figure 14, and an even smaller amount when going from Figure 14 to Figure 15. However, no spreading is visible

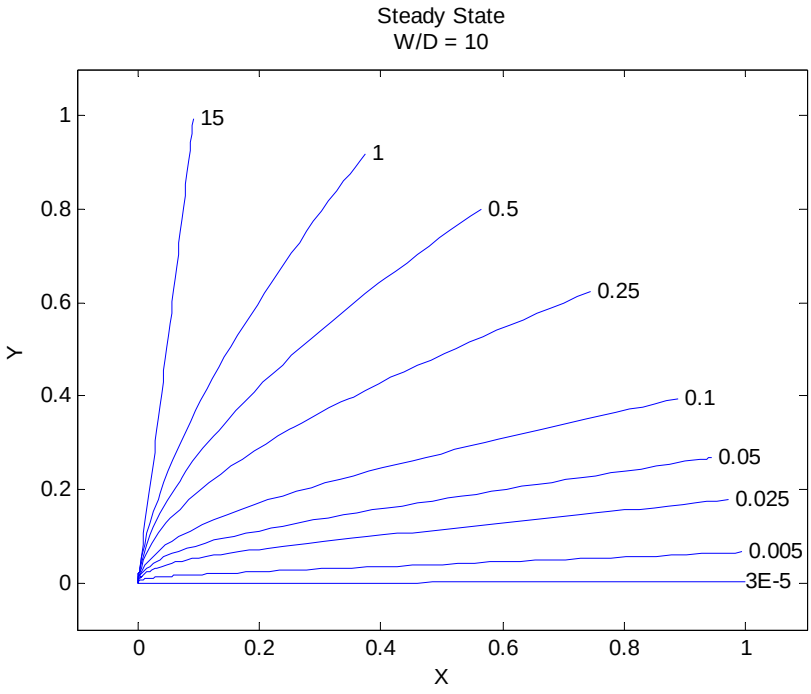

Figure 13. Towline Shapes with Decoy Drag to Weight Ratio = 10

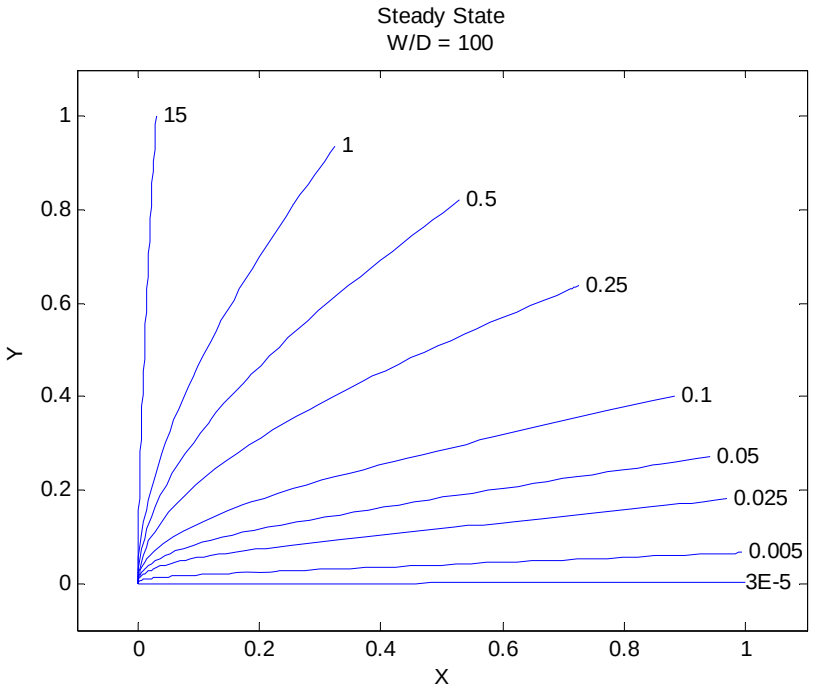

Figure 14. Towline Shapes with Decoy Drag to Weight Ratio = 100

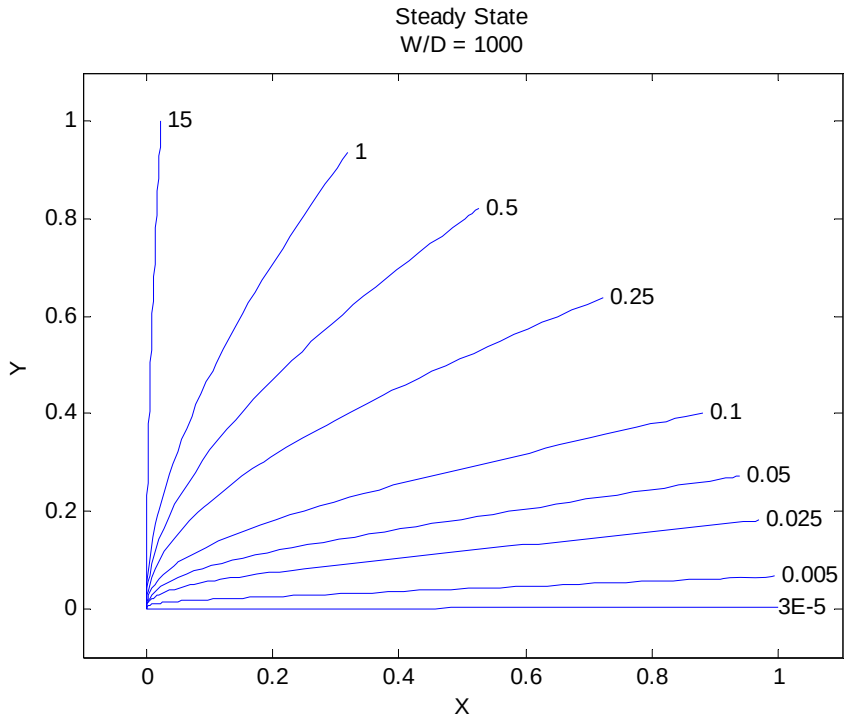

Figure 15. Towline Shapes with Decoy Drag to Weight Ratio = 1000

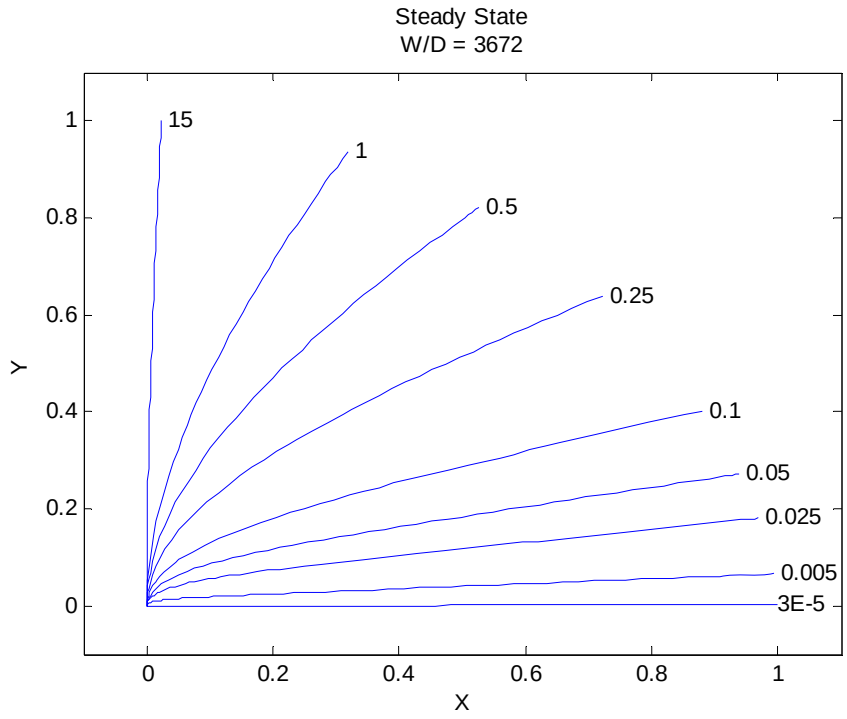

Figure 16. Towline Shapes with Decoy Drag to Weight Ratio = 3672

between the last two plots, as the lines on Figure 15 and Figure 16 are nearly identical and indistinguishable. All the plots generated in this study are available in Appendix B. Figures showing the towline shapes produced with *decoy weight to drag ratios* in between the ratios displayed in the text can be found there, as well as the figures included in the text.

Error Analysis

Since the plots of the towline shapes were produced using the results of numerical integration, the shapes are only as accurate as the numerical solver. The default settings for the tolerances of *ode45* were used in this work. Those settings are 1E-3 for the

relative error tolerance and 1E-6 for the absolute error tolerance. The relative error tolerance is the number of correct digits in the solution. Typically, a Runge-Kutta routine iterates until the solution is changing by less than this tolerance. The absolute error tolerance is the threshold under which the relative error tolerance does not need to be met (i.e. as the solution goes to zero). By using the default settings, the solutions in this work had three correct digits after the decimal point. With the equations nondimensionalized, this equates to an error of less than 0.1% of the towline length in the towline shapes.

V: Conclusions and Recommendations

This thesis identified groups of parameters that affect the shape of the towline of an aircraft decoy during a steady state condition of straight and level flight. The effect of each group was also determined and will be discussed next. This work can serve as a resource of towline shapes as many illustrations for the range of values of the groups are provided. The results can also be interpreted to formulate ways to prevent the towline from drifting into the exhaust plume of the aircraft engine. Future work will be able to provide greater detail about the system by solving the transient case and monitoring the movement of the towline during maneuvers.

The important groups of parameters for the steady state case are the *body force group*

$$\frac{\rho_t \pi d_t}{2 \rho_a V^2} g$$

and the *decoy weight to drag ratio*

$$\frac{W_D}{D_{Dx}}$$

These two groups are responsible for determining the shape of a towline of an aircraft decoy towed behind an aircraft flying straight and level. Regardless of what the values are of the individual parameters making up the groups, if the group as a whole has a certain value the towline shape will always be predicted as the appropriate shape illustrated in one of the figures in Chapter IV or Appendix B. For example, if the *body force group* had a value of 0.5, and then the diameter of the towline was doubled (numerator) but so was the density of air (denominator) by flying at a lower altitude, the

value of the group would remain 0.5 and the towline shape would stay the same. Along the same lines, the doubling of a value in the numerator, such as the diameter of the towline, would have the same effect as halving a value in the denominator, like the density of air.

One parameter that drops out of the groups that intuitively seems like it would have an effect on the system is the length of the towline. Based on the results of this research, however, it does not have an effect on the steady state case. On the other hand, the length of the towline does remain in the *acceleration group* and will have an influence in the transient case where the *acceleration group* must be included because the time derivatives will be nonzero.

The *decoy weight to drag ratio* determines how widespread the towline shapes can be, or how obtainable a nearly vertical towline is. In all cases of the *decoy weight to drag ratio*, values at the lower end of the *body force group* range predicted a towline to be horizontal out the back of the aircraft. However, only in the cases with a high value for the *decoy weight to drag ratio* could a nearly vertical towline be predicted for the highest values of the *body force group*. This is not to say that a vertical towline is desired, this is only offering a description of what the *decoy weight to drag ratio* determines.

If the *decoy weight to drag ratio* determines what towline shapes are obtainable, then the *body force group* determines what shape the towline will form within the obtainable range. In all cases, low values for the *body force group* meant horizontal or nearly horizontal towlines. The high values of the *body force group* predicted towline shapes at the limit determined by the *decoy weight to drag ratio*, whether this was a

gentle downward sloping shape predicted with a low *decoy weight to drag ratio*, or a nearly vertical, steep downward slope predicted at high *decoy weight to drag ratios.*

It appears that a relationship exists between the two parameter groups that determines the curvature of the towline shape. When the ratio of the *body force group* to the *decoy weight to drag ratio* is greater than one, meaning the *body force group* is larger than the *decoy weight to drag ratio*, the towline shape exhibits positive curvature. When the *body force group* is less than the *decoy weight to drag ratio,* and their ratio is less than one, the towline has negative curvature.

The desired towline shape and operational environment should be taken into consideration when designing the towed decoy system. For example, we already know that when the towline gets in the aircraft engine exhaust it may be damaged, so a horizontal towline shape is not desired. This study shows that low values for both the *decoy weight to drag ratio* and especially the *body force group* should be avoided to prevent this problem during straight and level flight. At the same time, we should be hesitant to conclude that the highest values for these two groups should be used as well. With high values the towline hangs nearly vertical. If the operational environment includes low flight altitudes a decoy hanging well below the aircraft would not be useful because it could potentially hit trees or other things on the ground. Then again, maybe the decoy isn't towed at low altitudes and there may be benefits to a low hanging decoy during maneuvers. The research of the transient case would be useful here to determine how a nearly vertical towline responds during maneuvers.

As of right now, a safe design appears to have values of the *body force group* and the *decoy weight to drag ratio* somewhere in the middle of the ranges of the two groups.

For the *body force group* this could be values between 0.025 and 0.25 and for the *decoy weight to drag ratio* this could be values from 0.1 to 5. One more design consideration should be examined, the question of positive or negative curvature. If curvature matters, then the system can be designed to have the desired ratio between the two groups. It seems reasonable to claim that positive curvature is better than negative curvature, since more of the towline of one with negative curvature extends out horizontally directly behind the aircraft than of one with positive curvature. The towline with negative curvature, staying higher longer with respect to the aircraft, has more of a chance of encountering the exhaust plume of the aircraft engine.

As a result of this research, it is possible to state that to help prevent the towline from entering the aircraft engine exhaust, the value of the *body force group* should be 0.025 or greater and the value of the *decoy weight to drag ratio* should be 0.1 or greater. It can also be speculated that a shape with positive curvature would be beneficial and to produce this kind of shape the *body force group* should be greater than the *decoy weight to drag ratio*.

These conclusions and recommendations could be substantiated with future research in this area. Since the towing aircraft will not be limited to straight and level flight, the transient case needs to be investigated. This will allow aircraft maneuvers to be simulated in order to examine the responsiveness of the towline and to observe its movement relative to the aircraft. The influence of curvature on the movement of the towline should also be studied to know which kind to design for. Additionally, the transient case of the nearly vertical towline can be researched to determine if there is any benefit to having the towline as far away from the aircraft engine exhaust plume as

possible. The procedure described in Chapter III can be used as a building block to develop a solution to the transient case. The derivation of the equations included the three-dimensional transient terms and it wasn't until the implementation into the code provided in Appendix A that the assumptions were made and the time derivatives set to zero. A numerical integration routine for the system of differential equations needs to be written for the transient case. As noted earlier, for the transient case the direction of integration will need to be from the aircraft down to the decoy. Unfortunately, this direction of integration could not be implemented into the steady state case in this research due to suspected sensitivity to initial conditions.

By combining the results of this work with the results of the recommended future research, the range of values for the parameter groups that gives a towline that stays out of the engine exhaust plume and responds well during maneuvers can be determined. Then the towed decoy system can be designed to have those parameter group values during operation.

Bibliography

Ball, Robert E. *The Fundamentals of Aircraft Combat Survivability Analysis and Design, Second Edition.* Reston: American Institute of Aeronautics and Astronautics Inc., 2003.

Barnes, Burdette J., Jr. and John L. Pothier. *Wind Tunnel Measurement of Airborne Towed Cable Drag Coefficients.* MS thesis, AFIT/GA/MC/71-4. School of Engineering, Air Force Institute of Technology (AU), Wright-Patterson AFB OH, June 1971 (AD-754889).

Buckham, B., M. Nahon, and M. Seto. "Three-Dimensional Dynamics Simulation of a Towed Underwater Vehicle," *Proceedings of the 18th International Conference on Offshore Mechanics and Arctic Engineering,* 6: 91-98 (July 1999).

Hoerner, Sighard F. *Fluid-Dynamic Drag: Practical Information on Aerodynamic and Hydrodynamic Resistance.* Midland Park: Hoerner, 1965.

Kang, S.W. and V.R. Latorre. *Aerodynamics Modeling of Towed-Cable Dynamics.* Contract W-7405-Eng-48. Livermore CA: Lawrence Livermore National Laboratory, January 1991 (UCRL-ID-106509).

Narkis, Yahli. "Approximate Solution for the Shape of Flexible Towing Cables," *Journal of Aircraft,* 14: 923-925 (September 1977).

Schram, Jeffrey W. and Stanley P. Reyle. "A Three-Dimensional Dynamic Analysis of a Towed System," *Journal of Hydronautics,* 2: 213-220 (October 1968).

Skop, Richard A. and Choo, Young-Il. "The Configuration of a Cable Towed in a Circular Path," *Journal of Aircraft,* 8: 856-862 (November 1971).

Appendix A: Towline Code

The following is the MATLAB® computer code used to integrate the system of differential equations and obtain the results in this research. The first function integrates the equations in the second function for one *body force group* value and one *decoy weight to drag ratio* and plots the towline shape.

```
function SSode_17
%ENS Tyler Richardson
%Thesis
%5/15/05
%Towed decoy system in STEADY STATE conditions
%Integrate from decoy up to the aircraft in terms of dl
%T0 = weight of cable

global group1

Wght_Drg = 0.09;          %decoy weight to drag ratio
group1 = 0.004;           %body force group

x0 = 0;                   %initial x-position
y0 = 0;                   %initial y-position
z0 = 0;                   %initial z-position
Ti = 1;                   %initial tension in towline
alpha0 = atan(Wght_Drg); %initial alpha
phi0 = 0;                 %initial phi
Li = 0;                   %initial length along towline

initial = [x0; y0; z0; Ti; cos(alpha0); sin(alpha0)*cos(phi0); sin(alpha0)*sin(phi0)];
      %create vector of initial conditions

[x, y] = ode45(@f_towline_c, [0 1], initial);
   %use ode45 to integrate the equations in f_towline_c, starting at a
   %dl of 0 and going to a dl of 1, with the initial conditions above

n = length(y(:,4));     %determine number of steps in integration
figure(2)
plot(y(:,1),y(:,2))     %plot xy-plane
title({'Steady State';['W/D = ',num2str(Wght_Drg)]})
xlabel('X')
ylabel('Y')
text(y(n,1),y(n,2),[' ',num2str(group1)])
axis([-0.1 1.1 -0.1 1.1])
```

```
function f = f_towline_c(x,y)
%ENS Tyler Richardson
%Thesis
%5/15/05
%function (f) to be integrated with respect to dl
%from the decoy up to the aircraft
%equations assume STEADY STATE conditions (no transients)

global group1

group2 = group1;            %T0 = weight of the cable, group2 = group1
Cd = 1.1;                   %coefficient of drag of the towline
Ds = 0.04;                  %skin friction drag on towline

sina = sqrt(y(6)^2 + y(7)^2);                   %definition of sin(alpha)
dl = sqrt((y(5))^2 + (y(6))^2 + (y(7))^2);      %dl^2 = (dx^2 + dy^2 + dz^2)

T = y(4);           %Tension in towline
dx = y(5);
dy = y(6);
dz = y(7);

f(1,1) = y(5);      %dx/dl
f(2,1) = y(6);      %dy/dl
f(3,1) = y(7);      %dz/dl
f(4,1) = (Ds*dx + 2*Cd*dx*dz^2*sina + dy*group2) / (group1*(dl^2));
    %dT/dl
f(5,1) = (Ds*(sina^2) + Cd*sina*(dx^2*(dy^2 - dz^2) + (sina^2)^2) - dx*dy*group2) / ((dl^2)*group1*T);
    %d2x / dl^2
f(6,1) = (-Ds*dx*dy - Cd*dx*dy*(sina)*(dx^2 + dy^2 + 3*dz^2) + ...
   (dx^2 + dz^2)*group2) / ((dl^2)*group1*T);
    %d2y / dl^2
f(7,1) = (-Ds*dx*dz + Cd*dx*dz*(dx^2 + dy^2 - dz^2)*sina - dy*dz*group2) / ((dl^2)*group1*T);
    %d2z / dl^2
```

This third function is the code used to generate the plots in the text and Appendix B with multiple towline shapes on each figure.

```
function SSode_data_f
%ENS Tyler Richardson
%Thesis
%5/10/05
%Integrate from decoy up to the aircraft in terms of dl
%use to collect data at widest ranges of the nondimensional groups
%multiple towline shapes plotted on one figure
%each figure represents a different decoy weight to drag ratio value
%each towline shape represents a different body force group value
%Group1 = Group2
```

```
clear all

global group1

i = 0;  %initialize counter
GRP1 = [3E-5 0.005 0.025 0.05 0.1 0.25 0.5 1 15];
   %range of body force group
W_D_ratio = [1.6E-4 0.005 0.05 0.1 0.2 0.3 0.4 0.5 2/3 0.75 1 1.25 1.5...
   1.75 2 2.5 3 4 5 10 100 1000 3672];
   %range of decoy weight to drag ratio

for k = 1:length(W_D_ratio)        %cycle through range of decoy weight
   Wght_Drg = W_D_ratio(k);        %to drag ratio

   i = i + 1;
   figure(i)                    %open figure

   for j = 1:9                   %cycle through body force group range
      x0 = 0;                   %initial x-position
      y0 = 0;                   %initial y-position
      z0 = 0;                   %initial z-position
      Ti = 1;                   %initial tension in towline
      alpha0 = atan(Wght_Drg);    %initial alpha angle
      phi0 = 0;                  %initial phi angle
      group1 = GRP1(j);          %assign body force group

      initial = [x0; y0; z0; Ti; cos(alpha0); sin(alpha0)*...
         cos(phi0); sin(alpha0)*sin(phi0)];
         %vector of initial conditions at decoy end

      [x, y] = ode45(@f_towline_b, [0 1], initial);
         %use ode45 to integrate differential equations in f_towline_b
         %from dl = 0 to dl = 1, with initial conditions above

      n = length(y(:,1));     %determine number of integration steps

      plot(y(:,1),y(:,2))     %plot xy-plane
      title({'Steady State';['W/D = ',num2str(Wght_Drg)]})
      xlabel('X')
      ylabel('Y')
      if j == 1
         text(y(n,1),y(n,2),'3E-5')
      else
         text(y(n,1),y(n,2),[' ',num2str(group1)])
            %include body force group value at end of towline plot
      end
      axis([-0.1 1.1 -0.1 1.1])
      hold on
   end
end
```

Appendix B: Plots of Towline Shapes

The following plots display all the towline shapes generated in this work.

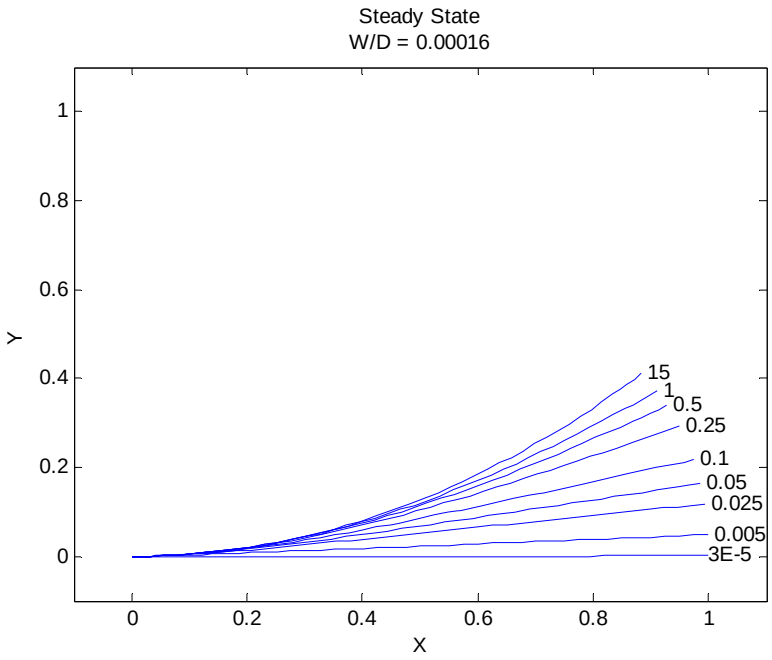

Figure 17. Towline Shapes with Decoy Drag to Weight Ratio = 1.6E-4

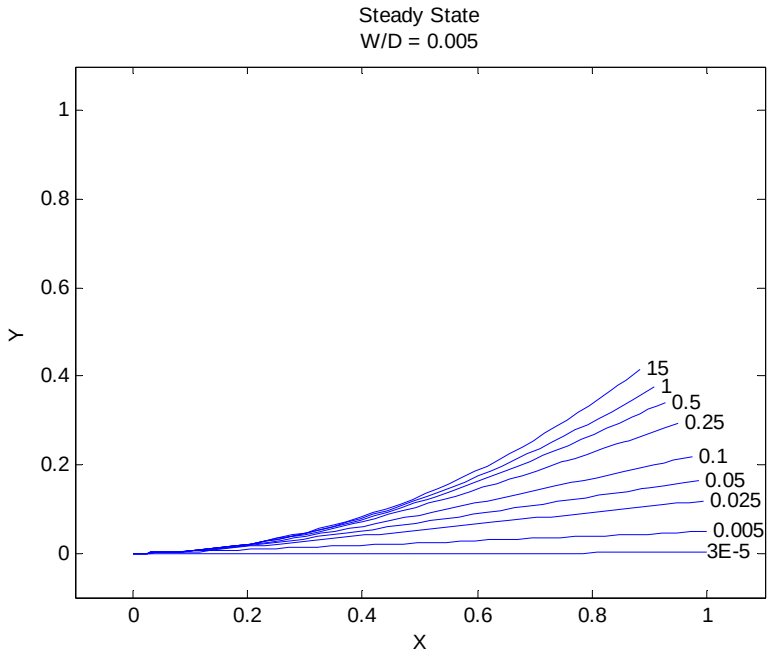

Figure 18. Towline Shapes with Decoy Drag to Weight Ratio = 0.005

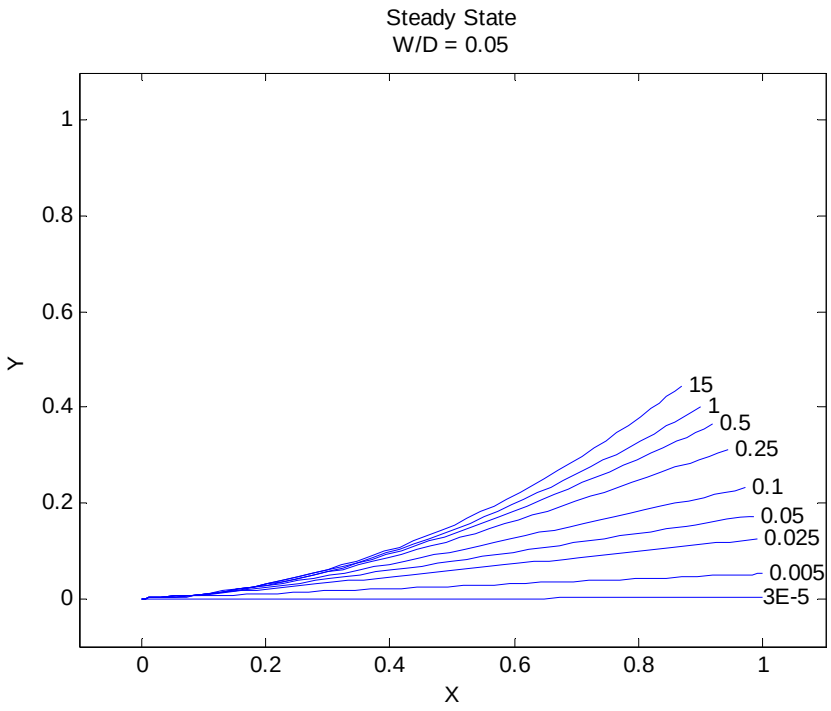

Figure 19. Towline Shapes with Decoy Drag to Weight Ratio = 0.05

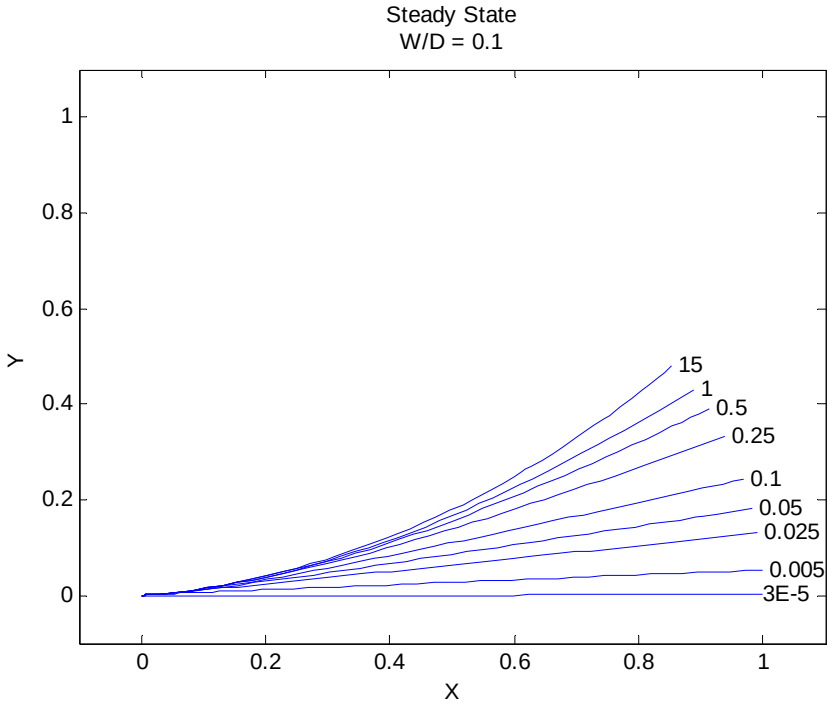

Figure 20. Towline Shapes with Decoy Drag to Weight Ratio = 0.1

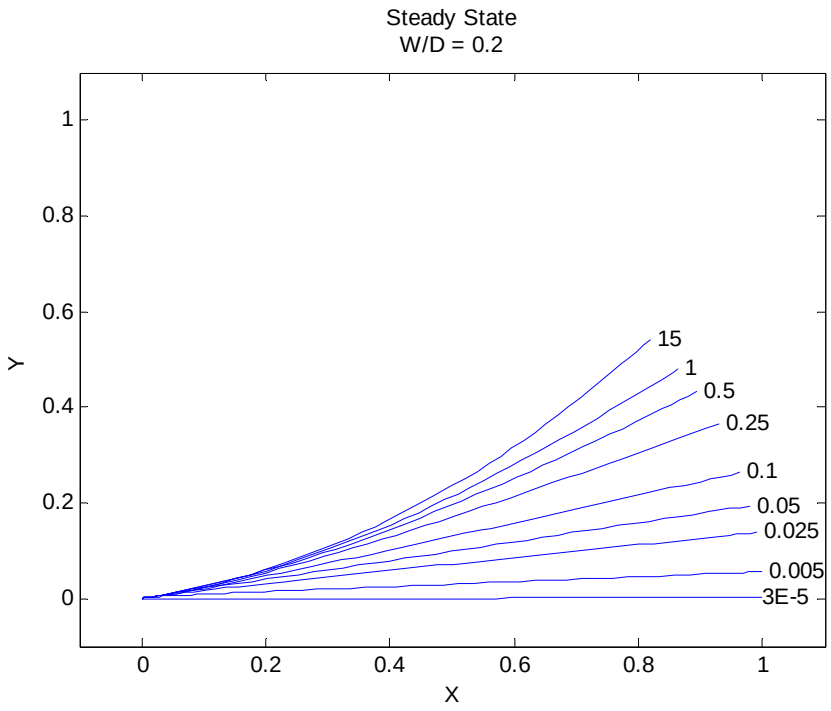

Figure 21. Towline Shapes with Decoy Drag to Weight Ratio = 0.2

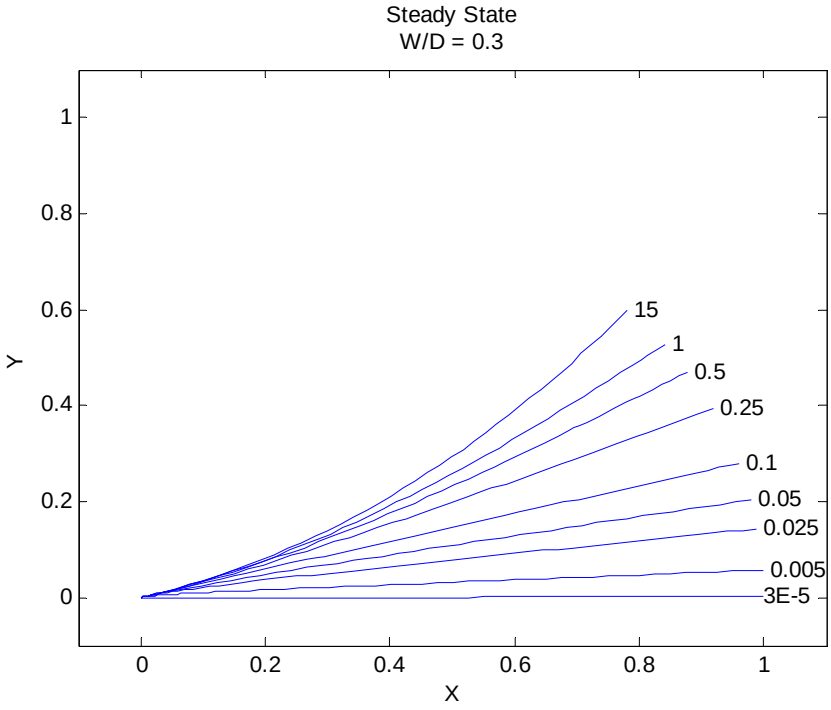

Figure 22. Towline Shapes with Decoy Drag to Weight Ratio = 0.3

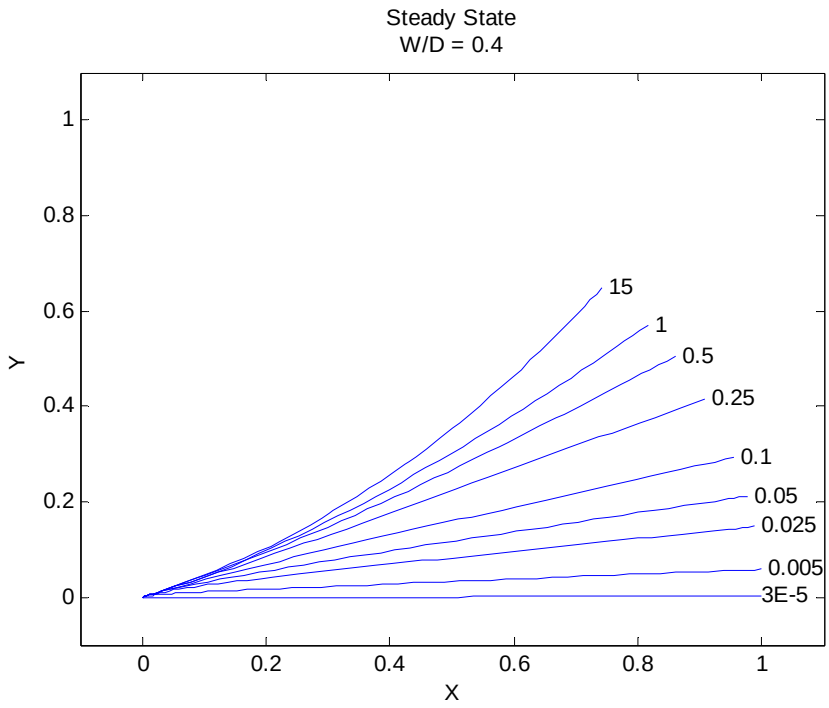

Figure 23. Towline Shapes with Decoy Drag to Weight Ratio = 0.4

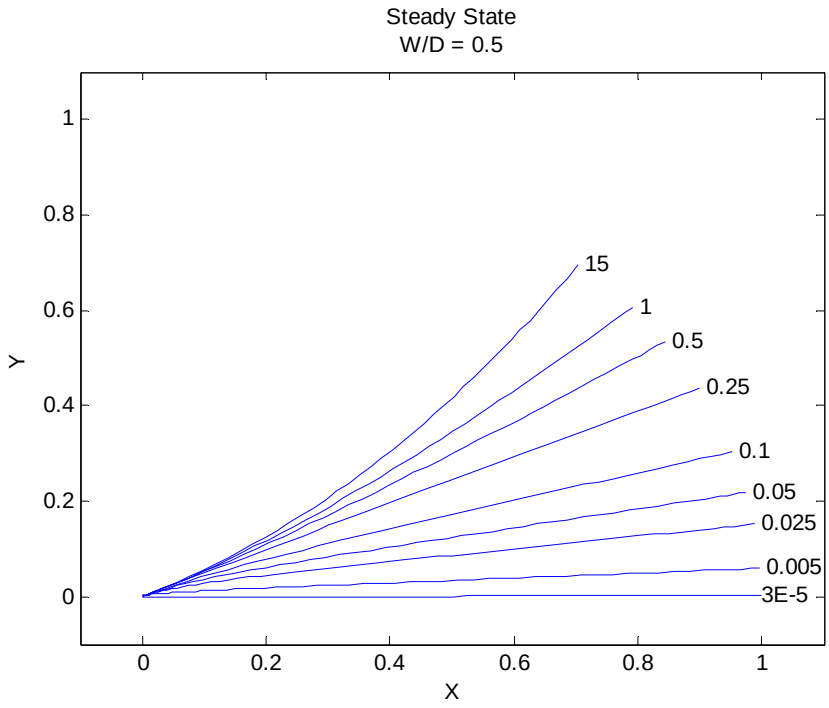

Figure 24. Towline Shapes with Decoy Drag to Weight Ratio = 0.5

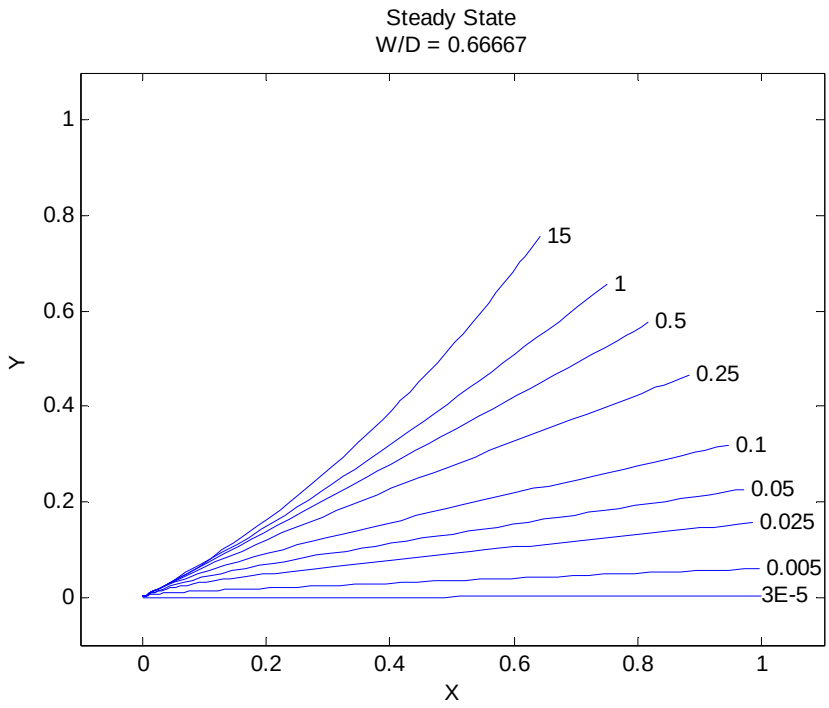

Figure 25. Towline Shapes with Decoy Drag to Weight Ratio = 0.667

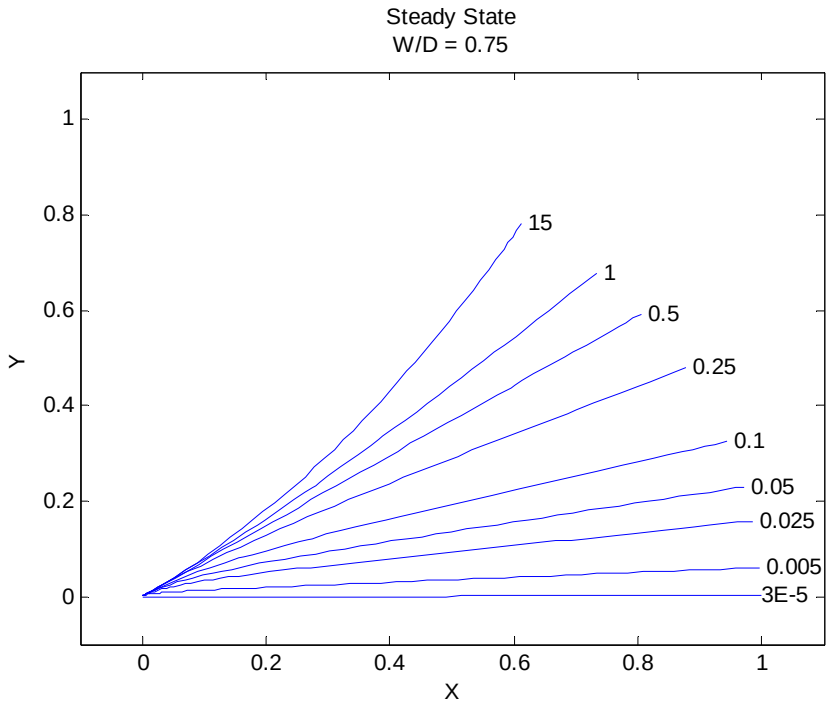

Figure 26. Towline Shapes with Decoy Drag to Weight Ratio = 0.75

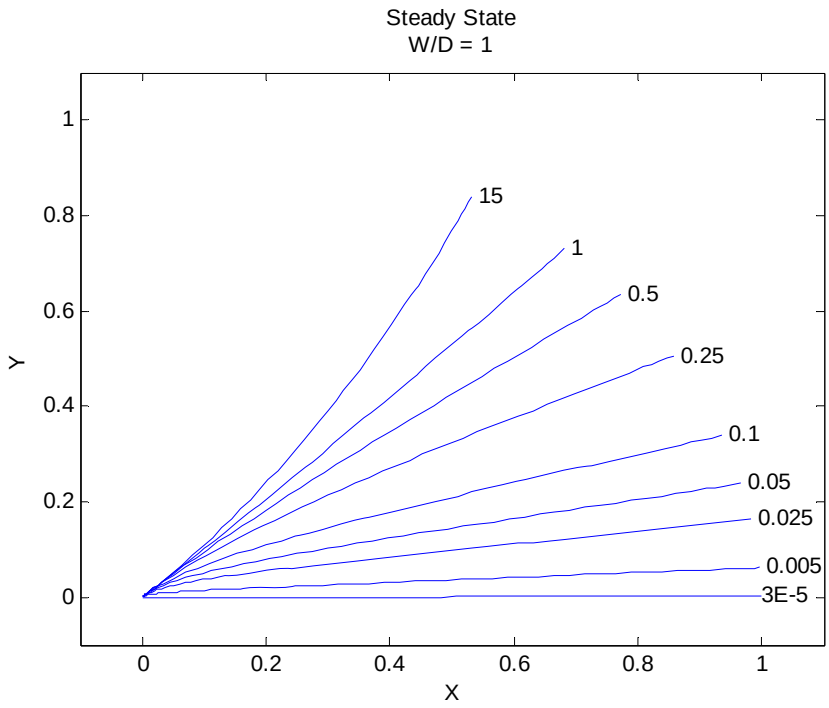

Figure 27. Towline Shapes with Decoy Drag to Weight Ratio = 1

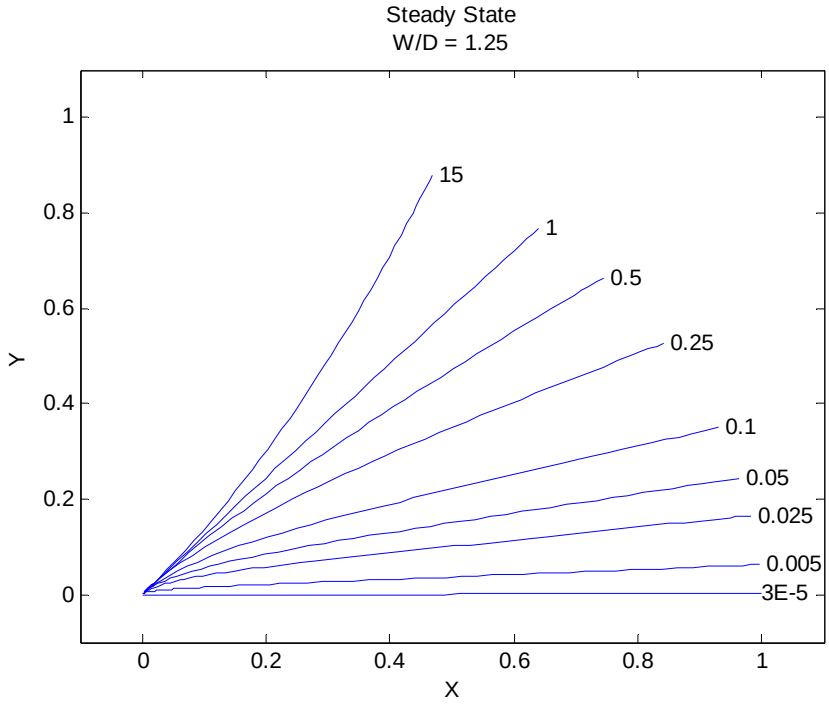

Figure 28. Towline Shapes with Decoy Drag to Weight Ratio = 1.25

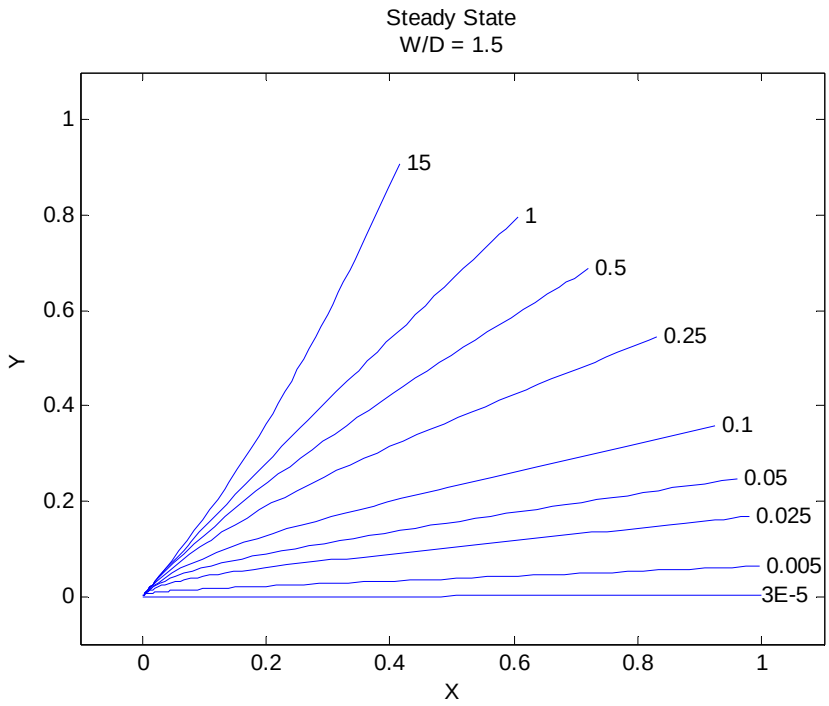

Figure 29. Towline Shapes with Decoy Drag to Weight Ratio = 1.5

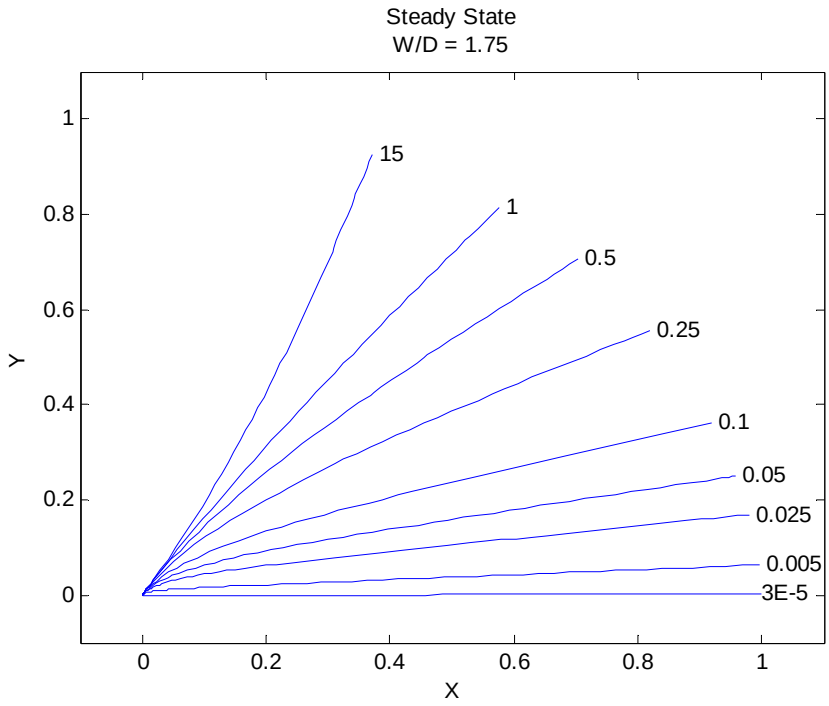

Figure 30. Towline Shapes with Decoy Drag to Weight Ratio = 1.75

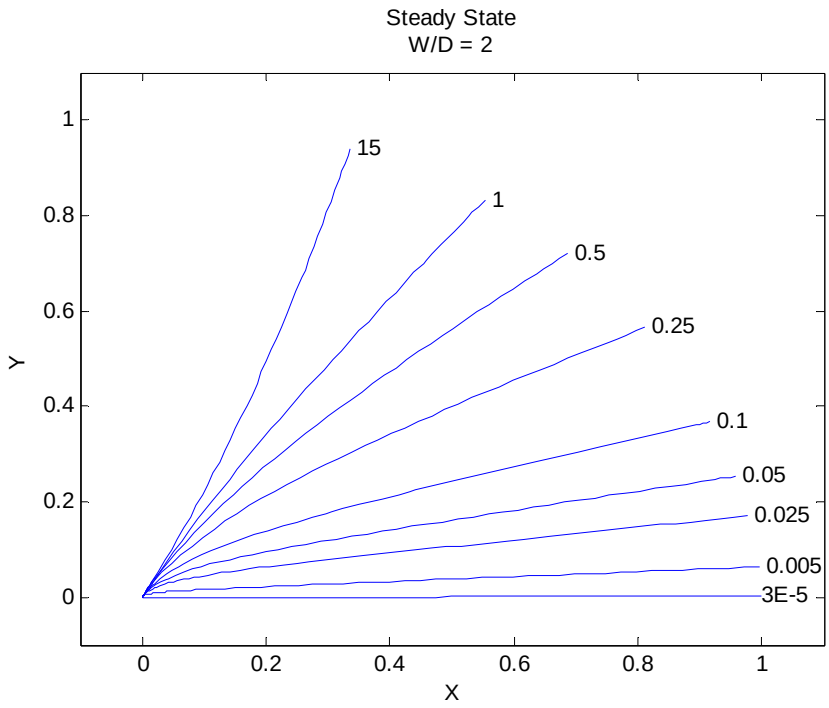

Figure 31. Towline Shapes with Decoy Drag to Weight Ratio = 2

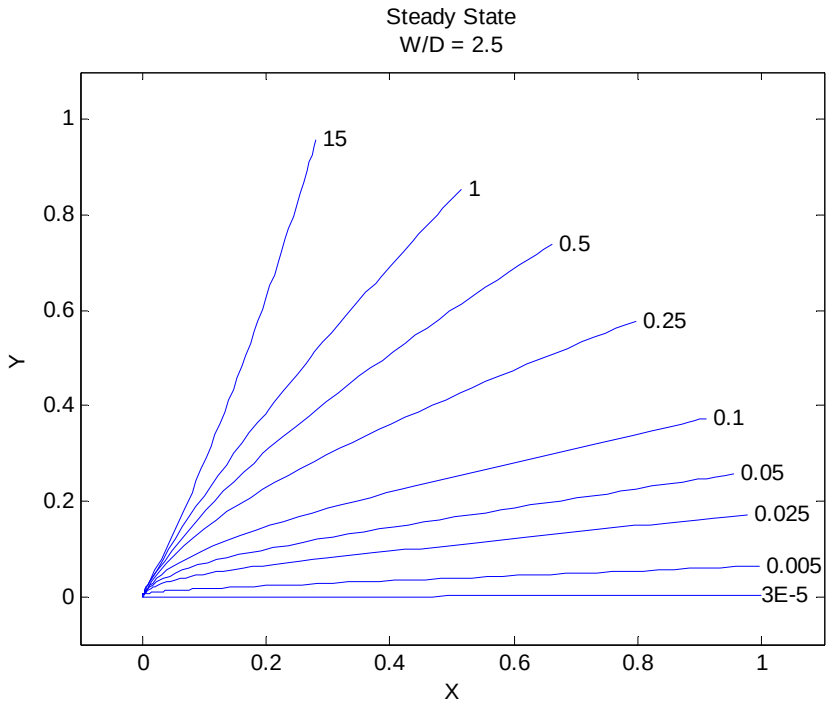

Figure 32. Towline Shapes with Decoy Drag to Weight Ratio = 2.5

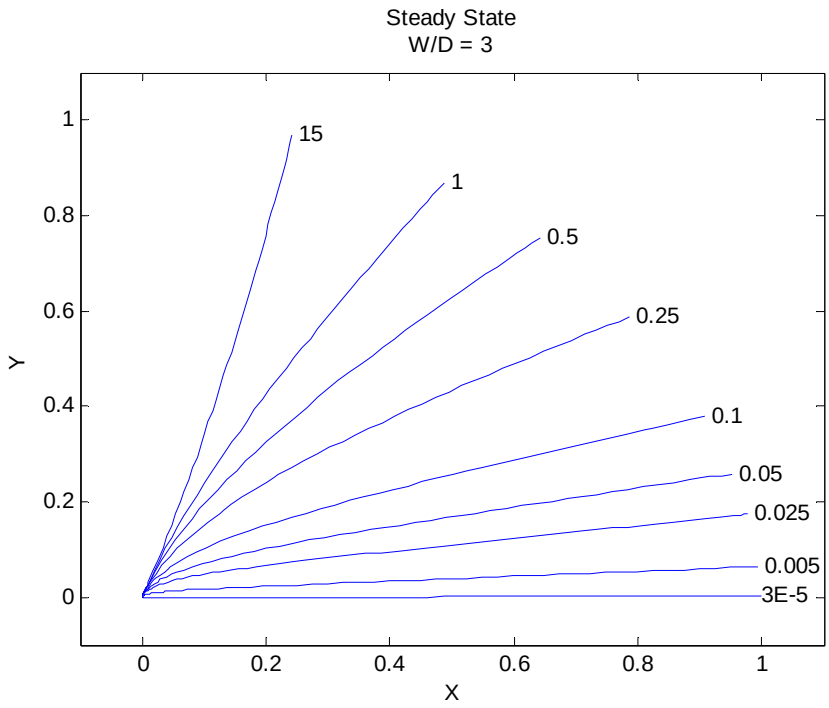

Figure 33. Towline Shapes with Decoy Drag to Weight Ratio = 3

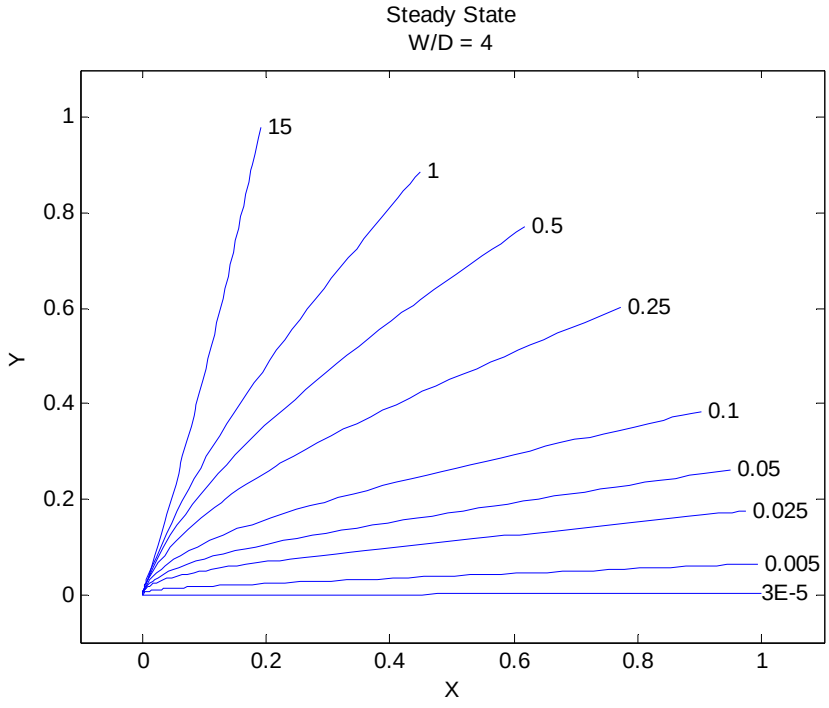

Figure 34. Towline Shapes with Decoy Drag to Weight Ratio = 4

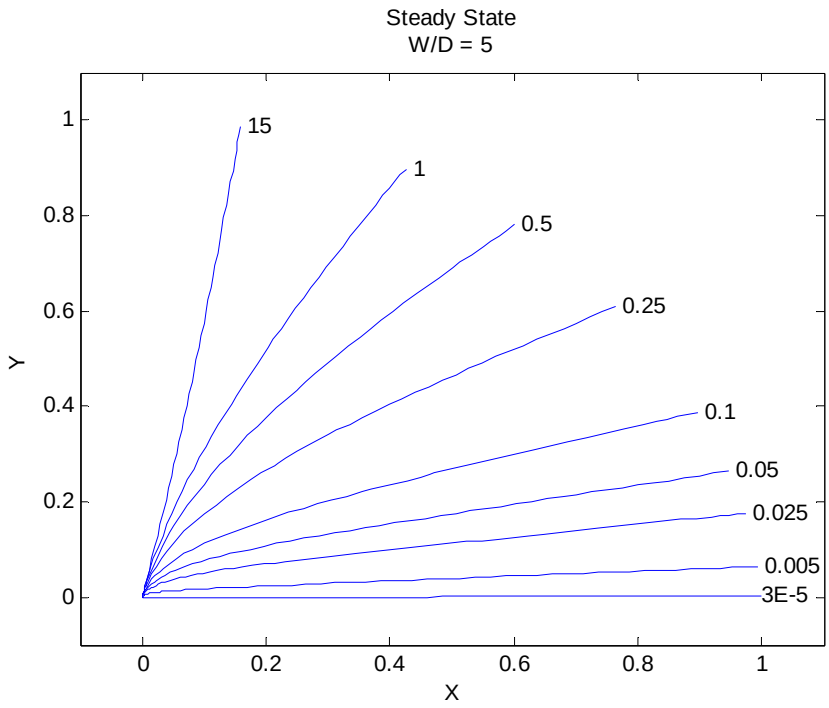

Figure 35. Towline Shapes with Decoy Drag to Weight Ratio = 5

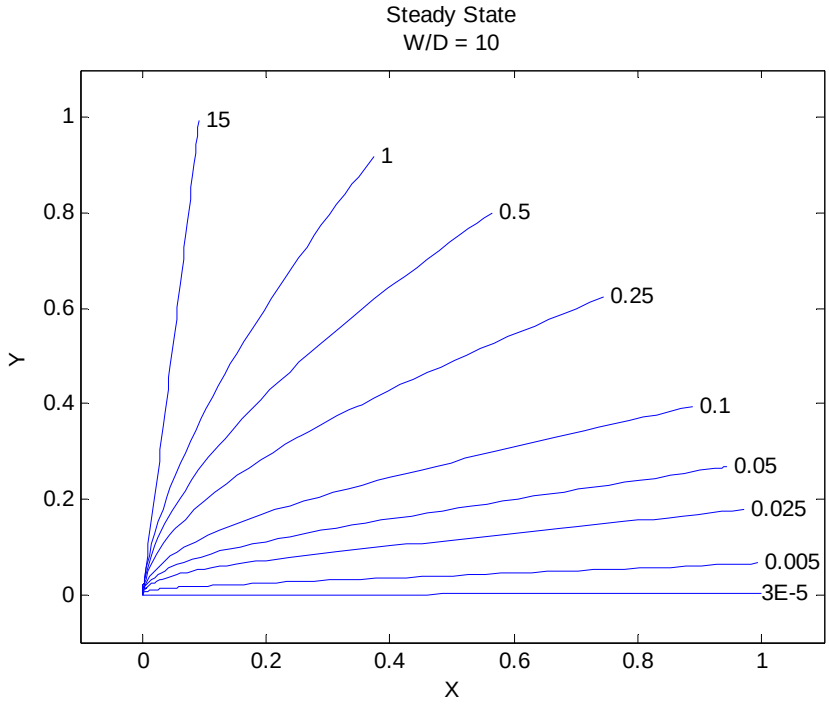

Figure 36. Towline Shapes with Decoy Drag to Weight Ratio = 10

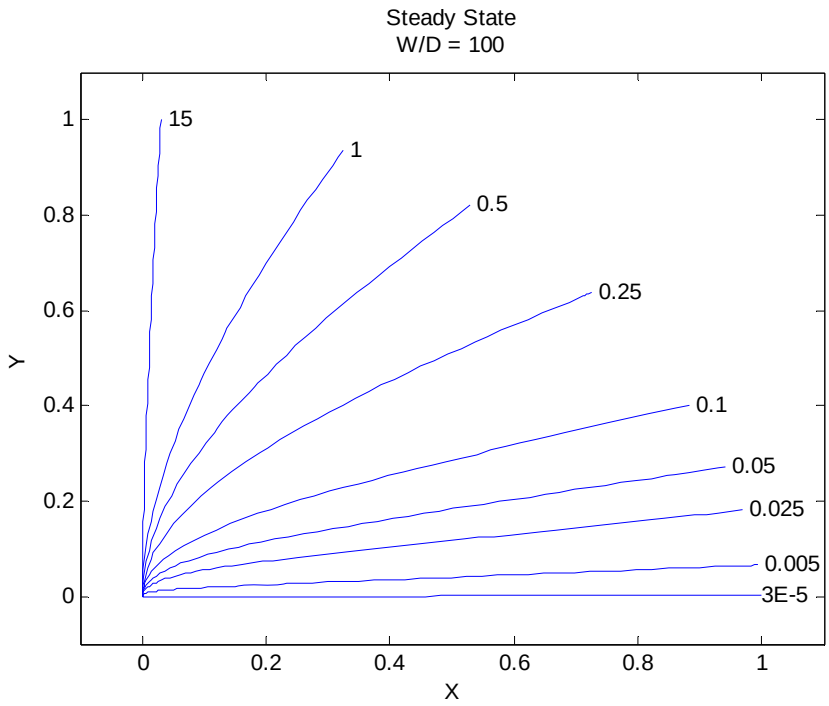

Figure 37. Towline Shapes with Decoy Drag to Weight Ratio = 100

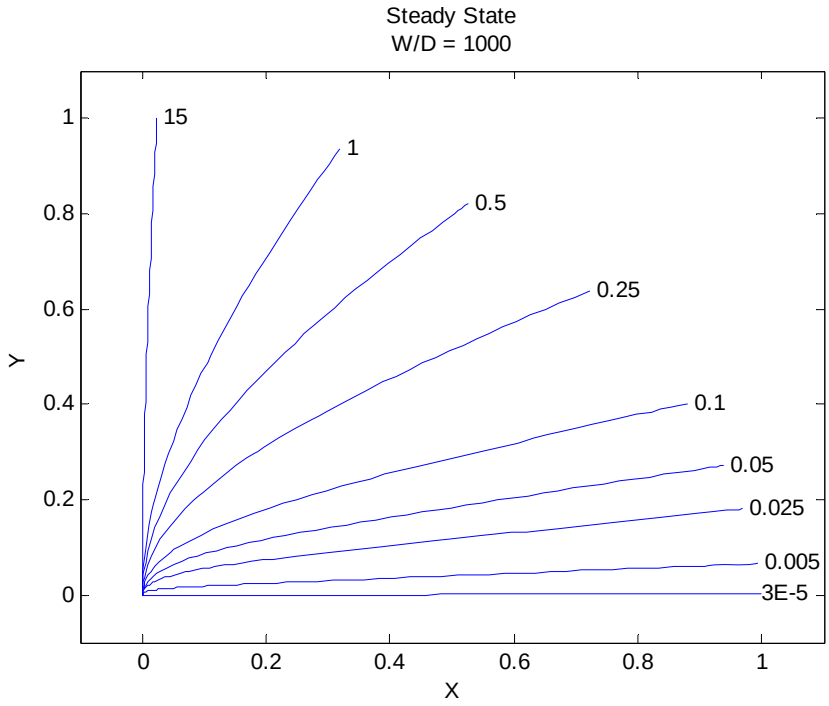

Figure 38. Towline Shapes with Decoy Drag to Weight Ratio = 1000

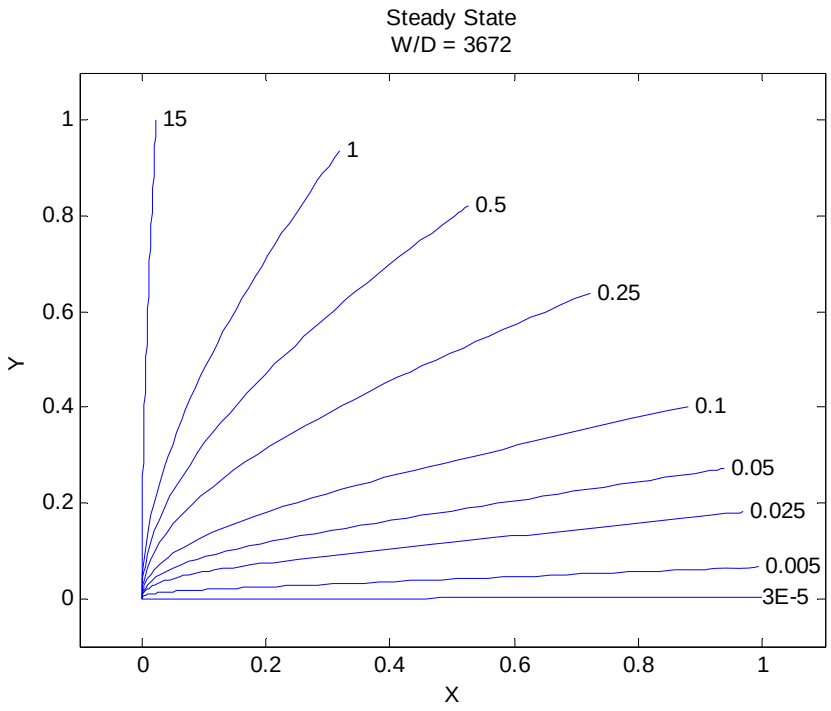

Figure 39. Towline Shapes with Decoy Drag to Weight Ratio = 3672

Vita

Ensign Tyler L. Richardson graduated from Coloma High School in Coloma, Michigan in May 2000. He entered undergraduate studies at the University of Michigan, where he graduated with a Bachelor of Science in Engineering degree in aerospace engineering in May 2004. He was commissioned through the NROTCU at the University of Michigan. His first assignment was at the Graduate School of Engineering and Management, Air Force Institute of Technology, upon which he entered in June 2004. Upon graduation in June 2005, he will be assigned to NAS Pensacola, FL to begin flight training.

REPORT DOCUMENTATION PAGE

Form Approved
OMB No. 074-0188

1. REPORT DATE *(DD-MM-YYYY)*	**2. REPORT TYPE**	**3. DATES COVERED** *(From – To)*
13-06-2005	**Master's Thesis**	01 OCT 04 – 13 JUN 05

4. TITLE AND SUBTITLE

Parametric Study of the Towline Shape of an Aircraft Decoy

5a. CONTRACT NUMBER

5b. GRANT NUMBER

5c. PROGRAM ELEMENT NUMBER

6. AUTHOR(S)

Richardson, Tyler L., Ensign, USNR

5d. PROJECT NUMBER

5e. TASK NUMBER

5f. WORK UNIT NUMBER

7. PERFORMING ORGANIZATION NAMES(S) AND ADDRESS(S)

Air Force Institute of Technology
Graduate School of Engineering and Management (AFIT/EN)
2950 Hobson Way
WPAFB OH 45433-7765

8. PERFORMING ORGANIZATION REPORT NUMBER

AFIT/GAE/ENY/05-J08

9. SPONSORING/MONITORING AGENCY NAME(S) AND ADDRESS(ES)

ASC/AANA
Attn: Mr. Randall Becknell
2145 Monahan Way
WPAFB, OH 45433-7017

10. SPONSOR/MONITOR'S ACRONYM(S)

11. SPONSOR/MONITOR'S REPORT NUMBER(S)

12. DISTRIBUTION/AVAILABILITY STATEMENT

APPROVED FOR PUBLIC RELEASE; DISTRIBUTION UNLIMITED.

13. SUPPLEMENTARY NOTES

14. ABSTRACT

Some of today's aircraft use decoys as a defense against enemy weapons. The decoy is towed behind the aircraft with the intention of attracting the weapon propagator by deception, trying to mislead the weapon into detecting it instead of the aircraft. An aircraft deploys a decoy via a towline extending out behind and below the aircraft. However, during some maneuvers, the towline moves up into the jet exhaust plume of the aircraft. The high temperatures of the exhaust can cause damage to the towline cable, ranging from disrupting data flow between the decoy and aircraft to severing the towline altogether. This research modeled the system to determine the towline shape and position relative to the aircraft under steady state conditions. Non-dimensional parameters were utilized in order to investigate what parameter groups effect the motion of the towline, reducing the steady state solution space from 7 parameters to 2 parameters. The effect of both parameter groups in determining the shape of the towline was studied, and recommendations for preventing the towline from entering the jet exhaust during straight and level flight were made.

15. SUBJECT TERMS

Towline, Towed Cable, Aircraft Decoy, Aircraft Survivability, Cylinder Drag

16. SECURITY CLASSIFICATION OF:			**17. LIMITATION OF ABSTRACT**	**18. NUMBER OF PAGES**	**19a. NAME OF RESPONSIBLE PERSON**
REPORT	**ABSTRACT**	**c. THIS PAGE**			Dr. Ralph Anthenien, AFIT/ENY
U	**U**	**U**	**UU**	80	**19b. TELEPHONE NUMBER** *(Include area code)* 937-255-3636 rantheni@afit.edu

Standard Form 298 (Rev: 8-98)
Prescribed by ANSI Std. Z39-18